Temperature Dependence of the HO_2 + ClO Reaction. 1. Reaction Kinetics by Pulsed Photolysis-Ultraviolet Absorption and *ab initio* Studies of the Potential Surface.

Scott L. Nickolaisen[1], Coleen M. Roehl[2], Lisa K. Blakeley[3], Randall R. Friedl[4], Joseph. S. Francisco[5], Ruifeng Liu[6] and Stanley P. Sander[*]

[1] Department of Chemistry & Biochemistry, California State University, Los Angeles, CA 90032
[2]Jet Propulsion Laboratory, California Institute of Technology, Pasadena, CA 91109
present address: Division of Geological and Planetary Sciences, California Institute of Technology, Pasadena, CA 91125
[3] Department of Chemistry & Biochemistry, California State University, Los Angeles, CA 90032
present address: Department of Chemistry, University of California, Irvine, CA 92697
[4]Jet Propulsion Laboratory, California Institute of Technology, Pasadena, CA 91109
[5] Department of Chemistry and Department of Earth and Atmospheric Sciences
Purdue University, West Lafayette, IN 47907
[6]Department of Chemistry, East Tennessee State University, Johnson City, TN 37614
[*]Jet Propulsion Laboratory, California Institute of Technology, Pasadena, CA 91109. Also with the Division of Geological and Planetary Sciences, and Division of Engineering and Applied Science, California Institute of Technology, Pasadena, CA 91125. Author to whom correspondence should be addressed.
email: ssander@jpl.nasa.gov fax: (818) 393-5019

Abstract

The kinetics of the HO_2 + ClO reaction was studied using the flash photolysis/ultraviolet absorption technique over the temperature range 203-364 K and pressure range 50-700 Torr of N_2. In contrast to previous work, the temperature dependence displayed linear Arrhenius behavior over the entire temperature range with the rate constant being described by the expression $k(T) = 2.84 \times 10^{-12} \exp\{(312\pm60)/T\}$ cm^3 molecule^{-1} s^{-1}. *Ab initio* calculations of intermediates and transition states have been carried out on the singlet and triplet potential energy surfaces. These calculations show that the reaction proceeds mainly through the ClO-HO_2 complex on the triplet surface; however, collisionally stabilized HOOOCl formed on the singlet surface will possess an appreciable lifetime due to large barriers toward decomposition to HCl and HOCl. Termolecular rate calculations using *ab initio* parameters lead to a strong collision rate constant of ~ 5×10^{-32} cm^6 molecule^{-2} s^{-1} for HOOOCl formation. This intermediate may be important under both laboratory and atmospheric conditions.

Submitted to the Journal of Physical Chemistry

Introduction

According to a recent international assessment of stratospheric ozone, the most current two-dimensional model calculations underestimate the observed trend in lower stratospheric ozone by a factor of two or more[1]. This region of the atmosphere (14-24 km. altitude) is characterized by chemical and dynamical processes that are strongly coupled. While this complicates the analysis, there is a strong suspicion that these trends are attributable to increases in anthropogenic halogen-containing compounds that destroy stratospheric ozone by catalytic mechanisms. In the lower stratosphere at midlatitudes the most important catalytic cycles for ozone destruction are the ones for which the reactions

$$ClO + HO_2 \rightarrow HOCl + O_2 \quad (1)$$

$$BrO + HO_2 \rightarrow HOBr + O_2 \quad (2)$$

$$BrO + ClO \rightarrow \text{products} \quad (3)$$

are the rate-limiting steps.[2,3]. While there has been considerable experimental work on the BrO + HO_2 and BrO + ClO reactions under stratospheric conditions in recent years[4-6], there has been relatively little work on the ClO + HO_2 reaction. In particular, there has been only one study of the temperature dependence of the overall rate coefficient in the last twenty years.[7]. This study obtained nonlinear Arrhenius behavior leading to the suggestion that the reaction mechanism is dominated by hydrogen-abstraction above 298 K and complex formation at lower temperatures.

The idea that complexes can play a role in the pressure and temperature dependence phenomenology of the HO_2 + ClO reaction has been reinforced by recent thermochemical and *ab initio* studies of $HClO_3$ intermediates[7-15]. Stimpfle *et al.* proposed the cyclic elimination of HOCl from HOOClO and possibly HCl from HOOOCl intermediates as reaction pathways at low temperature. Mozurkewich[8] was able to reproduce the negative temperature dependence observed by Stimpfle *et al.* using two-channel RRKM calculations. He concluded that there would be large barriers for cyclization of HOOOCl and HOOClO and that the reaction proceeded primarily through a hydrogen-bonded intermediate on the triplet surface. Buttar and Hirst[12] carried out calculations at the MP2 level of theory for both singlet and triplet surfaces. They

proposed a complex mechanism for the singlet surface which involved a 1,2-hydrogen shift from HOOOCl to form HOCl + O_2. Francisco and Sander[15] carried out extensive MP4 calculations, obtaining the energy ordering of the $HClO_3$ singlet isomers. This work showed that HOOOCl was the most stable isomer accessible from HO_2 + ClO reactants, followed by HOOClO. None of these studies calculated the energetics of the transition states and therefore the barriers for product formation.

In this study, the flash photolysis-ultraviolet absorption technique has been used to study the HO_2 + ClO reaction over the temperature range 203-364 K and pressure range 50-700 Torr. To minimize possible systematic errors associated with secondary reactions, two different photolytic schemes were used for reactant production. Extensive *ab initio* calculations of the structures and energetics of $HClO_3$ intermediates and transition states were carried out using coupled-cluster and density functional methods. The results are used to interpret the observed pressure and temperature dependence behavior of the reaction kinetics.

Experimental

The flash photolysis/long path length UV/vis absorption apparatus has been described previously.[16] The photolysis cell is based on a concentric design with a temperature control jacket, xenon flash lamp, light filter and reaction volume. Identical cells made of quartz (photolysis wavelength > 200 nm) and Pyrex (photolysis wavelength > 300 nm) were employed. A schematic of the experimental apparatus is shown in Figure 1.

Transient Absorption Spectrometry: For this experiment, several modifications were made to the optics of the long-path absorption system. Two analytical light sources were used: a 300 W xenon lamp optimized for wavelengths longer than 250 nm and a 150 W deuterium lamp optimized for the 200–250 nm spectral region. The beams from both lamps were collimated and coaligned along the probe beam axis using a dichroic beamsplitter. The combined probe beam was directed through an iris and into a reaction cell equipped with White-type optics. The total optical path length was 724 cm. Another dichroic beamsplitter divided the probe exit beam into

a 200-250 nm component and a $\lambda > 250$ nm component. The short wavelength component was directed into a 0.5 m monochromator with 500 μm slits (resolution 0.5 nm FWHM) used for HO_2 detection. The long wavelength component was further divided using a 50:50 dichroic beamsplitter into two beams directed into separate monochromators. A 0.3 m monochromator (150 μm slits, 0.3 nm FWHM) was set at the maximum of the ClO (A, v'=12 $\leftarrow$ X, v'=0, Ω = 3/2) subband transition at 275.2 nm, and a 0.25 m monochromator (150 μm slits, 0.3 nm FWHM) was set at the adjacent minimum at 276.4 nm. This arrangement permitted ClO detection with high selectivity using the differential absorption method. The proper alignment of the ClO detectors was verified by ensuring that the two ClO detection channels gave identical absorbance signals when both were tuned to the (12-0) ClO absorption maximum.

Photomultiplier outputs from the two ClO channels and the HO_2 channel were separately recorded and signal averaged using a 14-bit 100 kHz digital oscilloscope. Absorption signals were analyzed after averaging 100 shots. Absorbances for each data channel were derived from calculations of $\ln(I_o/I)$ where I was the time-dependent signal voltage following initiation of the reaction by the flash lamp, and I_o was determined by averaging about 80 pre-flash data points for each data channel. The ClO differential absorption signal was determined by subtracting the calculated absorbance for the 276.4 nm channel from the calculated absorbance for the 275.2 nm channel.

Radical Production: Two different chemical sources were employed for formation of the ClO and HO_2. In the first source, F_2-H_2-O_2-Cl_2O mixtures were photolyzed in the quartz cell with N_2 as the bath gas. The flash lamp photolyzed both F_2 and Cl_2O to initiate the reaction mechanism (all rate constants are from DeMore *et al.* [17] unless otherwise indicated):

$F_2 + h\nu\ (\lambda>220\ nm) \rightarrow 2\ F$

$F + H_2 \rightarrow HF + H$ $\qquad k(T) = 1.4 \times 10^{-10} \exp\{-500/T\}\ cm^3\ molecule^{-1}\ s^{-1}$

$H + O_2 + M \rightarrow HO_2 + M$ $\qquad k(T) = 5.7 \times 10^{-32} (T/300)^{-1.6}\ cm^6\ molecule^{-2}\ s^{-1}$

$Cl_2O + h\nu\ (\lambda>220\ nm) \rightarrow ClO + Cl$

$\rightarrow O + Cl_2$

$Cl + Cl_2O \rightarrow ClO + Cl_2$ $\quad k(T) = 6.2 \times 10^{-11} \exp\{130/T\}$ cm^3 molecule^{-1} s^{-1}

In order to minimize the photolysis of O_2, the filter jacket of the quartz cell was filled with neat N_2O at a total pressure of 1 atm. The absorption of N_2O limited photolysis to $\lambda > 220$ nm. The effectiveness of the N_2O filter was verified by observing that O_3 production was negligible in the photolysis of pure O_2 which set an upper limit of 1×10^{-5} for the fraction dissociated in the quartz cell. Cl_2O was introduced into the reaction cell by flowing helium at 5 psia through a bubbler containing the Cl_2O sample. The bubbler was immersed in an *iso*-propanol/CO_2(s) slush at 196 K at which temperature the Cl_2O vapor pressure is about 5 Torr.

The photolysis of Cl_2O at wavelengths in the range 200-250 nm produces $O(^3P)$ with a quantum yield of 0.3 or less[5,18-20]. The primary loss process for the $O(^3P)$ will be through recombination with O_2 to form O_3. The resulting O_3 concentration will be somewhat more than 10% of the initial ClO concentration. At this level the contribution to the measured absorbances of HO_2 and ClO are negligible as are the effects associated with secondary reactions of O_3.

In the second reactant source, Cl_2-Cl_2O-CH_3OH-O_2 mixtures were photolyzed in the Pyrex cell with N_2 as the bath gas. The mechanism for HO_2 and ClO formation was

$Cl_2 + h\nu\ (\lambda > 300\ nm) \rightarrow 2\ Cl$

$Cl_2O + h\nu\ (\lambda > 300\ nm) \rightarrow ClO + Cl$

$Cl + Cl_2O \rightarrow ClO + Cl_2$ $\quad k(T) = 6.2 \times 10^{-11} \exp\{130/T\}$ cm^3 molecule^{-1} s^{-1}

$Cl + CH_3OH \rightarrow CH_2OH + HCl$ $\quad k(T) = 5.4 \times 10^{-11}$ cm^3 molecule^{-1} s^{-1}

$CH_2OH + O_2 \rightarrow HO_2 + CH_2O$ $\quad k(T) = 9.1 \times 10^{-12}$ cm^3 molecule^{-1} s^{-1}

Cl_2 was the only species photolyzed in the Pyrex cell. Cl_2O was handled in a manner identical to that used in the F_2-H_2-O_2-Cl_2O experiments. CH_3OH was introduced into the reaction cell by flowing helium at 5 psia through a bubbler containing the CH_3OH sample at 233 K. Chlorine (10% Cl_2 in helium), O_2 and N_2 were combined with Cl_2O and CH_3OH in the mixing manifold.

All reagents were mixed in a manifold prior to entering the reaction cell. Flows of all gases were measured with calibrated mass flowmeters, and concentrations were calculated from the measured flow rates and the cell temperature and pressure. The concentrations of reactants and

initial ClO and HO_2 concentrations are summarized in Table 1. In both the F_2-H_2-O_2-Cl_2O and Cl_2-Cl_2O-CH_3OH-O_2 experiments, HO_2 and ClO were formed on time scales which were much shorter than their loss by reaction 1 or by other reactions. The effect of secondary reactions on the reaction kinetics will be discussed in detail below.

Both chemical systems resulted in reproducible kinetic decays. The F_2-H_2 system had the advantage that $[ClO]_o$ and $[HO_2]_o$ could be controlled somewhat more easily than with the Cl_2-CH_3OH source because the two radicals had different precursors (Cl_2O and F_2, respectively). In the Cl_2-CH_3OH system the precursor is Cl_2 for both radicals. In the Cl_2-CH_3OH system, aerosol formation was observed under certain conditions. The onset of aerosol formation was a sensitive function of temperature and $[CH_3OH]$ and the time dependence of the aerosol extinction was highly reproducible at a fixed set of conditions. It was necessary to limit the range of initial radical concentrations that could be employed at temperatures below 235 K in order to avoid the aerosol formation. Aerosol was not observed in the F_2-H_2 system under any conditions.

Materials: The gases used in this study had the following stated purities and were used as supplied: 10% Cl_2 (99.5%) in He (99.9995%), 5% F_2 (>98%) in He (99.9999%), H_2 (99.9999%), O_2 (99.999%), He (99.9999%), Ar (99.9993%). CH_3OH (99.93%) was purified by several freeze/pump/thaw cycles. Cl_2O was synthesized by the method of Cady[21]. Ultraviolet and infrared analysis showed that the only impurity in the Cl_2O was Cl_2 at the level of 5% or less.

Ab Initio Computational Methods: All of the calculations presented here were performed with the GAUSSIAN 94 software package on the JPL Cray J90 supercomputer.[22] Searches for minima and saddle points employed the Becke's nonlocal three-parameter exchange with the Lee-Yang-Parr density functional (B3LYP) method,[23,24] with 6-31G(d,p) and 6-311++G(3df,3pd) basis sets. In the searches for the pathways for the HO_2 + ClO reaction, the linear synchronous transition state following method was used to obtain initial structures. No restrictions on symmetries were imposed on the initial structures, so that geometry optimizations for saddle points occurred with all degrees of freedom. All stationary points were characterized by harmonic vibrational frequency calculations. In addition, energies were calculated with the

coupled-cluster method, which included singles and doubles excitations, plus a perturbational estimate of the effects of connected triple excitations [CCSD(T)][25]. These energies were calculated with the 6-311++G(3df,3pd) basis set using the geometry obtained at the B3LYP/6-311++G(3df,3pd) level of theory.

Results

Spectrometry

The absorption spectra of several important species in the two chemical systems are shown in Figure 2 and an example of the time-dependent 210 nm and differential 275.2/276.4 nm signals is shown in Figure 3. The absorption at 210 nm is dominated by HO_2; however a number of other species contribute to the background absorbance at this wavelength. To a first approximation, these background absorptions do not change over the time scale of reaction 1 but cause a small step change in the measured absorbance immediately after the flash. For the fluorine system, the species contributing to the measured absorbance at 210 nm include Cl_2O, F_2, ClO, Cl_2O_2, H_2O_2, and HOCl. The latter four species are products of secondary reactions. For the chlorine system, the absorbers at 210 nm are ClO, Cl_2O_2, H_2O_2, and HOCl. For both chemical systems the time-dependent absorbance of each species was calculated by the computer program FACSIMILE[26] using the absorption cross sections listed in Table 2. The HO_2 cross section used in the model is taken from Maricq and Szente[27]. This value is somewhat lower than the NASA recommendation,[17] but provided excellent agreement with the literature value of the $HO_2 + HO_2$ rate coefficient when used in the fitting routine described below.

The expressions used in FACSIMILE to calculate the 210 nm absorbances for the fluorine and chlorine systems are given below:

$$A_{F_2}^{210}(t) = l\{\sigma_{HO_2}[HO_2] + \sigma_{Cl_2O_2}[Cl_2O_2] + \sigma_{H_2O_2}[H_2O_2] + \sigma_{HOCl}[HOCl] - \sigma_{F_2}([F_2]_o - [F_2]_t) - \sigma_{Cl_2O}([Cl_2O]_o - [Cl_2O]_t)\}$$

$$A_{Cl_2}^{210}(t) = l\{\sigma_{HO_2}[HO_2] + \sigma_{Cl_2O_2}[Cl_2O_2] + \sigma_{H_2O_2}[H_2O_2] + \sigma_{HOCl}[HOCl] - \sigma_{Cl_2O}([Cl_2O]_o - [Cl_2O]_t)\}$$

where l is the absorption path length and σ_i is the cross section of species i. The stoichiometry of the source reactions constrains the initial conditions for the numerical simulation, i.e.

$$[Cl_2O]_o - [Cl_2O]_t = [ClO]_o$$

and

$$[F_2]_o - [F_2]_t = \frac{1}{2}[F]_o$$

In both the fluorine and chlorine systems the contribution to the change in the 210 nm absorbance by species other than HO_2 is less than 7.5%.

For the two absorption channels near 276 nm, there are several species that contribute to the absolute absorbance including Cl_2O, Cl_2, ClO and F_2. Only ClO contributes to the *differential* absorbance due to its banded structure. The spectra of the other species are continua with relatively small differential cross sections. Room temperature ClO cross sections were taken from the work of Simon *et al.*[28] The temperature dependence of the ClO differential cross section was obtained from the expression

$$\sigma_{ClO}^{T} = \sigma_{ClO}^{298}\left\{1.011 - \frac{104.9}{T} + \frac{30330}{T^2}\right\}$$

where $\sigma_{ClO}(298\ K) = 4.10 \times 10^{-18}$ cm^2. This expression was determined by fitting the temperature-dependent ClO cross section data of Sander and Friedl[5] to an empirical equation.

As discussed below, the reaction mechanism for ClO + HO_2 may involve the formation of stable intermediates such as HOOOCl, particularly at low temperatures and high pressures. While it is doubtful that this species contributes to the differential absorbance at 275 nm, it is possible that there would be an interference with the HO_2 measurement at 210 nm. The effect of such an interference would be to cause the rate coefficient to be underestimated. Because the reaction proceeds mainly through channels that do not involve long-lived complex formation, and the concentration cannot exceed that of the minor species (ClO), it is unlikely that any such spectral interference will be significant.

Data Analysis

Analysis of the time-resolved decay profiles of HO_2 and ClO is complicated by several factors. While it is desirable to establish first-order conditions in excess HO_2 or ClO to minimize the sensitivity toward the absolute concentration of the minor species, this cannot be achieved in practice. While excess ClO conditions have the advantage that the ClO self-reaction is relatively slow, the formation of Cl_2O_2 at low temperatures causes significant spectral interference with the detection of HO_2 at 210 nm. Most of the experiments were therefore carried out with $[HO_2]_o/[ClO]_o$ in the range of 1-10. Because rate constants for $HO_2 + HO_2$ are within a factor of 3 of those for $ClO + HO_2$, the time scales for HO_2 and ClO disappearance were comparable, as shown in Figure 3. Since there is no simple analytic treatment of the resulting mixed first- and second-order kinetics, the data were analyzed numerically using FACSIMILE code. In this approach, rate constants are varied to obtain the best fit between the kinetic mechanism and the measured time-dependent absorption signals from the 210 nm and 275 nm channels. Separate mechanisms were used for the fluorine and chlorine systems. These mechanisms included all the reactions that had a significant effect on the formation and removal of ClO and HO_2.

The mechanism used in fitting the fluorine source chemistry data is given in Table 3. Four parameters were varied in the fitting procedure. These were the fractional dissociation of F_2 and Cl_2O from photolysis, and the rate coefficients for the $ClO + HO_2 \rightarrow HOCl + O_2$ and $HO_2 + HO_2 \rightarrow H_2O_2 + O_2$ reactions. By varying the initial F atom and ClO concentrations, FACSIMILE was able to fit the initial absorbances from both signal channels. The $HO_2 + HO_2$ rate coefficient was allowed to vary to obtain the best fit to the HO_2 decay profile. Values of the $HO_2 + HO_2$ rate coefficient calculated by this method were well within the uncertainty limits for this reaction as determined by DeMore *et al.*

The reaction mechanism used in the analysis of the chlorine system is given in Table 4. The four parameters varied in the fitting procedure were $[Cl]_o$ and rate coefficients for the ClO +

$HO_2 \rightarrow HOCl + O_2$, $HO_2 + HO_2 \rightarrow H_2O_2 + O_2$, and $Cl + Cl_2O \rightarrow ClO + Cl_2$ reactions. Cl_2 photolysis was the initiation step that produced both the ClO and HO_2 radicals. Variation of the rate constant for the $Cl + Cl_2O$ reaction provided the degree of freedom required to fit the initial absorbances in the 210 and 275 nm signal channels since this parameter affects the relative rates of HO_2 and ClO formation. The best-fit values of the $HO_2 + HO_2$ and $Cl + Cl_2O$ rate constants were typically within 25% of the accepted values[17]. Fitted decay profiles to experimental data from the F_2 and Cl_2 systems are shown as the solid lines in Figure 3.

The results of the rate constant measurements are summarized in Table 5. Data were obtained over the pressure range 25 – 600 Torr and temperature range 203 – 364 K. For each temperature and pressure, at least five runs were carried out varying the initial concentrations of ClO and HO_2. The averaged results for all data recorded using each reactant source mechanism are plotted in Arrhenius form in Figure 4. The results obtained with the Cl_2 source are consistently lower than those which used the F_2 source, but the differences lie well within the 2σ error limits. The Arrhenius plot is linear over the entire temperature range. The best fit to the data from both the F_2 and Cl_2 systems resulted in the following Arrhenius expression:

$$k_1(T) = 2.84 \times 10^{-12} \exp\{(312\pm60)/T\} \text{ cm}^3 \text{ molecule}^{-1} \text{ s}^{-1}$$

where the stated uncertainties are 2σ and include both random and systematic errors as discussed below.

The possible effect of pressure on the rate coefficient was examined by performing a series of room temperature measurements where the pressure was varied systematically between 50 and 700 Torr. No clear trend with respect to pressure could be observed. Because the lowest practical pressure attained in the experimental apparatus was 50 Torr, we cannot preclude the possibility of a pressure effect that is exhibited at lower pressures but reaches a high pressure limit near 50 Torr.

Discussion

Secondary Reactions:

Systematic errors in the determination of k_1 can arise primarily as a result of secondary reactions which form or remove ClO (the minor reactant) or through errors in the spectroscopic determination of the HO_2 concentration (the excess reactant). All of the known secondary reactions that can affect ClO production and loss have been incorporated into the kinetic model. The rate constants for these reactions were systematically varied to assess their sensitivity on the determination of k_1. Uncertainties in the spectroscopic measurement of ClO and HO_2 arising from imprecise measurement of baseline changes and absorption by other species were also assessed by this method.

A number of factors contributed to the rate coefficient uncertainties determined in the fitting process. The most significant of these were the uncertainties in the absorption cross sections and, to a lesser extent, the uncertainties in rate constants. The sensitivity of the fits to each of these factors was determined by randomly selecting a number of data sets that encompassed a range of temperatures, pressures, and initial reactant concentrations. FACSIMILE runs were performed as described previously, but with the value of an individual rate constant or cross section altered by the reported uncertainty in its literature value. The effect on k_1 is reported as a percent difference in Table 6. This was repeated for all parameters that were not varied within the fitting procedure. Table 6 lists the rate constants and cross sections whose uncertainties resulted in a corresponding uncertainty for k_1 that was larger than 0.1%.

The two reactions that had the largest effect on the fitted value of k_1 involved the formation and dissociation of the ClO dimer. This was true particularly under conditions of low temperature and/or high pressure where dimer formation competes more successfully with ClO + HO_2 for removal of ClO. Overall, these two reactions resulted in an uncertainty in k_1 of up to 4%. Uncertainties in rate constants involving other secondary reactions had a negligible effect on the determination of k_1.

As expected, the derived value of k_1 is also sensitive to the absorption cross section of HO_2 at 210 nm. A ±10% change in σ_{HO_2} resulted in a ±9% change in k_1. The fits also displayed a small sensitivity to the differential cross section of ClO at 275.2 nm and to the 210 nm absorption cross section of H_2O_2. In the case of the 275.2 nm ClO cross section, the measured rate coefficient was relatively independent of the ClO reactant concentration because experiments were typically performed under conditions with excess HO_2. As a result, derived values of k_1 were relatively insensitive to the ClO differential cross section. The combined effect of uncertainties in cross sections and rate coefficients results in a ±13% uncertainty in the fitted values for k_1.

Comparison with Previous Studies:

Rate constants for the HO_2 + ClO reaction have been measured several times at 298 K [7,29-32] and once over the temperature range 235-393 K.[7]. The results of these studies have been discussed extensively by DeMore *et al.*[17] and Atkinson *et al.*[33]. The published room temperature results lie in the range $(3.8\text{-}6.5)\times10^{-12}$ cm^3 $molecule^{-1}$ s^{-1}. The temperature dependence results of Stimpfle *et al.* displayed non-linear Arrhenius behavior with the data showing essentially no dependence on temperature above 298 K and a temperature dependence (E_a/R) of -700 K below 298 K. The current recommendations of both the NASA[17] and IUPAC[33] data evaluation panels are based on an average of the results from the 298 K studies combined with the temperature dependence below 298 K from Stimpfle *et al.* As shown in Figure 4, the results from the present study show linear Arrhenius behavior over the 203-364 K temperature range with a fitted value of E_a/R that is smaller than that of Stimpfle *et al.* Also shown in Figure 4 are the results of a recent temperature dependence study from this laboratory which uses the discharge-flow/mass spectroscopy technique[34]. The results from this experiment give a near-zero temperature dependence over the range 233-380 K ($E_a/R = 72 \pm 42$ K) and a value of k_{298} that is smaller than the previous studies.

Ab Initio Calculations of Reaction Pathways

Geometries and Vibrational Frequencies for Intermediates and Transition States

Singlet surface: In order to make sense of the negative temperature dependence of the overall rate coefficient and the observation of O_3 formation at low temperatures[35] it is necessary to understand the structures and energies of the reaction intermediates and transition states. Francisco and Sander[15] explored the possible isomers of $HClO_3$ that can result from the HO_2+ClO reaction on the singlet potential energy surface. Of the four structures located at potential energy minima, only HOOOCl and HOOClO can be formed as nascent products of the HO_2 + ClO reaction. The structures of these two species were calculated previously by Buttar and Hirst[12] at the MP2/6-31G** level of theory and by Francisco and Sander[15] at the MP2/6-31G* and MP2/6-311G(2df,2p) levels of theory. In the present study, the geometries of HOOOCl and HOOClO were reexamined at the B3LYP/6-311++G(3df,3pd) level of theory. These structures are presented in Table 7. Like the earlier studies, we find that the minimum energy structures for HOOOCl and HOOClO have skewed straight chain geometries. The HOOO′ dihedral angle for HOOOCl is 77.9° at both the MP2/6-311G(2df,2p) and the B3LYP/6-311++G(3df,3pd) levels of theory. The OOO′Cl dihedral angle at the MP2/6-311G(2d,2p) level of theory is 79.3°, while at the B3LYP/6-311++G(3df,3pd) level of theory it is 82.5°. The minimum energy structure for HOOClO has dihedral angles of 93.8° for the HOOCl group and 78.2° for the OOClO′ group at the MP2/6-311G(2d,2p) level of theory. At the MP2/6-311G(2df,2p) level of theory the HOOCl dihedral angle remains the same while the OOClO′ dihedral angle decreases to 72.3°. At the B3LYP/6-311++G(3df,3pd) level of theory, these angles are 92.2° and 80.1°, respectively. These results suggest that the B3LYP/6-311++G(3df,3pd) geometries are reasonable and compare well with MP2/6-311G(2df,2p) results.

The key reactions on the singlet HO_2 + ClO reaction surface that are considered in the present work are:

$$HO_2 + ClO \rightarrow HOCl + O_2 (^1\Delta)$$

$\rightarrow HCl + O_3$

More specifically, we have considered whether these products can be produced from the HOOOCl and HOOClO intermediates. We have located three transition states corresponding to the pathways $HOOClO \rightarrow HOCl + O_2 (^1\Delta)$, $HOOOCl \rightarrow HOCl + O_2 (^1\Delta)$, and $HOOOCl \rightarrow HCl + O_3$. The geometric parameters for the three transition states are given in Table 7, and the structures are illustrated in Figure 5a-c.

The $HO_2 + ClO$ pathway that proceeds through the HOOClO intermediate to form $HOCl + O_2 (^1\Delta)$ involves a five-center transition state. This transition state is illustrated in Figure 5a. The transition state is a non-planar structure. Comparing the OCl bond distance in the transition state and in the HOOClO intermediate, we find that the OCl bond in the transition state is significantly elongated (2.282Å for the transition state compared with 1.503Å for the intermediate). The OO bond length decreases from 1.422Å in the intermediate to 1.306Å in the transition state. The HO bond length increases from 0.969Å to 1.027Å. Intrinsic reaction coordinate (IRC) calculations show that transition state connects the intermediate (HOOClO) to the products ($HOCl + O_2 (^1\Delta)$). As shown in Table 8, vibrational frequency calculations show that the transition state is a first-order saddle point because there is one imaginary frequency.

The reaction pathway that proceeds through the HOOOCl intermediate to form $HOCl + O_2 (^1\Delta)$ involves a four-center transition state. This transition state is illustrated in Figure 5b. This transition state is a non-planar structure. The HOOO′ dihedral angle is –32.5°, showing that the hydrogen is considerably twisted out of the OOO plane. However, we note that the HOOO′ dihedral angle in the transition state is significantly different from that in the HOOOCl intermediate. The OO bond length is significantly shorter in the transition state (1.288Å) than in the intermediate (1.423Å) and the OO′ bond length in the intermediate (1.387Å) is also elongated relative to the transition state (2.282Å).

The other pathway by which the HOOOCl intermediate can proceed is through the products $HCl + O_3$. This pathway passes through a five-center transition state, as illustrated in Figure 5c. This transition state is non-planar, as well. The OH and ClO′ bonds are significantly elongated

relative to the HOOOCl intermediate. The OOO′ angle in the transition state is also between the angle for the HOOOCl intermediate (OOO′ = 108.8°) and ozone (OOO = 118.3°). Vibrational frequency calculations given in Table 8 show that the transition state structure is a first-order saddle point. Given the magnitude of the imaginary frequency for this transition state, i.e. 1106i, tunneling may play a role for this pathway.

Triplet Surface: In addition to exploring the reaction pathways on the singlet surface, the HO_2 + ClO reaction was also examined on the triplet surface. In these searches, two levels of theory were used to explore the reaction pathways. UMP2/6-31G(d) was used in the preliminary search. Once a transition state was found, a vibrational frequency calculation was performed to confirm that the structure was a first-order saddle point. The Hessian from the UMP2/6-31G(d) calculation was then used to search for the transition state at the CCSD(T)/6-31G(d) level of theory. Geometries from these two searches are given in Figure 6.

Hydrogen abstraction by ClO from HO_2 on the triplet surface correlates to ground-state $O_2(^3\Sigma)$ and HOCl. The reaction is found to proceed on the $^3A''$ surface and gives the correct orientation for the hydrogen abstraction. This is consistent with the calculations of Toohey and Anderson[9]. From the relative energies in Table 9, the complex is estimated to be bound by 2.8 kcal mol^{-1} at the CCSD(T)/6-311++G(2df,2p) level of theory. The complex is formed in the *cis* configuration (Figure 6a). As the ClO continues its approach toward the hydrogen, it can remain in the *cis* configuration (Figure 6b) or rotate into a *trans* conformation (Figure 6c). We find that the transition state in the *trans* conformation has a barrier of 0.7 kcal mol^{-1} above the HO_2 + ClO reactant level. On the *cis*- approach the barrier is 2.4 kcal mol^{-1} below the HO_2 + ClO reactant level. These results suggest that there is a fork at the entrance channel for the HO_2 + ClO reaction on the $^3A''$ surface. The most favorable orientation for hydrogen abstraction is via the *cis* approach. The heat of reaction for the HO_2 + ClO → HOCl + $O_2(^3\Sigma)$ reaction is estimated as -47.1 kcal mol^{-1} at the CCSD(T)/6-311++G(2df,2p) level of theory. There is a difference of 1.6 kcal mol^{-1} between the calculated and experimental heat of reaction. We find that this difference is similar to the rms difference in energy between the experimental and CCSD(T)/6-

311++G(3df,3pd) results of 1.2 kcal mol^{-1} for the singlet surface. The uncertainties in the results in Table 11 for the energetics for the triplet surface are about ± 3 kcal mol^{-1}.

Energetics of Reaction Pathways for the HO_2 + ClO Reaction

The total energies for reactants, products, intermediates and transition states are given in Table 10. Relative energies of all the species along both reaction channels are given in Table 11. It can be seen from Table 11 that the B3LYP/6-311++G(3df,3pd) and CCSD(T)/6-311++G(3df,3pd) results are consistent with available experimental results. The rms difference in energies between the experimental and CCSD(T)/6-311++G(3df,3pd) results is about 1.2 kcal mol^{-1}. A more reasonable estimate in the uncertainty in the calculated results is ±3 kcal mol^{-1} at the CCSD(T)/6-311++G(3df) level of theory. The relative energies for the reaction of HO_2 + ClO on the single surface are also presented schematically in Figure 7. The reaction of HO_2 + ClO to produce the HOOClO intermediate is estimated to be nearly thermoneutral ($\Delta H_{r,0}$ = -0.02 kcal mol^{-1}). The barrier to the products HOCl + O_2 ($^1\Delta$) from the HOOClO intermediate is calculated to be 4.3 kcal mol^{-1} at the CCSD(T)/6-311++G(3df,3pd) level of theory. If the reaction proceeds by the HOOOCl intermediate, the reaction is exothermic by 15.4 kcal mol^{-1}, but the formation of the products HOCl + $O_2(^1\Delta)$ has to proceed through a barrier that is 24.5 kcal mol^{-1} above the HOOOCl intermediate. This implies that there is a barrier that is 9.1 kcal mol^{-1} above the level of the HO_2 + ClO reactants.

The reaction channel leading to HCl + O_3 through the HOOOCl intermediate has a 22.7 kcal mol^{-1} barrier. Even though the HO_2 + ClO reaction to produce the HOOOCl intermediate is exothermic by 15.4 kcal mol^{-1}, there is a 7.3 kcal mol^{-1} barrier above the total reactant energy for this channel. This channel should be energetically forbidden, but considering the size of the imaginary frequency for the transition state for the HOOOCl→HCl+O_3 channel, tunneling should play an important role in the kinetics and the rate may be non-negligible. Several previous experiments either failed to observe O_3 as a product or could attribute its formation to secondary reactions thereby setting an upper limit of 2% or less for the HCl + O_3 branching ratio [36,30,37]. In

contrast, Finkbeiner *et al.* concluded that secondary reactions could not account for all the O_3 observed in their static photolysis/matrix-FTIR experiment and that the branching ratio is 5 ± 2 % at 210 K and 2 ± 1 % at 240 K [35]. This experiment was carried out at a total pressure of 700 Torr implying some stabilization of the HOOOCl intermediate under these conditions.

HOCl can be produced from the HO_2 + ClO reaction by both singlet and triplet pathways. On the triplet surface, the reaction occurs via direct abstraction of hydrogen by ClO from HO_2. Toohey and Anderson [38] have explored the transition state for this channel and found a barrier of 5.3 kcal mol^{-1} at the UMP4/6-31G** level of theory. We have also reexamined this process at the CCSD(T)/6-311++G(2df,2p) level of theory and find that the barrier falls below the reactant level by 2.4 kcal $mole^{-1}$, with a weakly bound hydrogen bonded complex that is formed. The complex is bound by 2.8 kcal mol^{-1} below the HO_2 + ClO reactants. Therefore, the formation of HOCl should occur by direct H atom abstraction on the triplet surface. On the singlet surface, the calculated barriers are sufficiently large to preclude the formation of HOCl at temperatures relevant to the atmosphere.

The results of previous *ab initio* calculations of the enthalpy of formation of HOOOCl are compared in Table 12. Neglecting the group additivity estimate of Stimpfle *et al.* and the MP2 results of Buttar and Hirst the average value of ΔH_f^o(298 K) from *ab initio* calculations is 11.4 ± 3.6 kcal mol^{-1} . The present work is the first high level *ab initio* calculation of the transition state energies. Grela and Colussi[39] estimated a barrier for the HOOClO reaction to form the products HOCl + O_2. Using MNDO, they estimated an overall barrier for the HO_2 + ClO reaction to be 9.8 kcal mol^{-1}. This value is in fair agreement with the results obtained here.

Pressure Dependence of the HO_2 + ClO → HOOOCl Pathway

As discussed in the previous section, the formation of HOCl + O_2 or HCl + O_3 on the singlet surface at atmospheric temperatures is unlikely because of the large energy barriers on these pathways. Because HOOOCl is bound by about 15 kcal mol^{-1} with respect to decomposition to reactants and about 25 kcal mol^{-1} with respect to product formation, this

species may be long-lived on the experimental time scale. The formation of HOOOCl is therefore expected to be pressure-dependent. The low-pressure limiting rate constant for the association reaction can be estimated using the theory of Troe [40,41] as developed by Patrick and Golden [42] and the NASA Panel for Data Evaluation [17]. This method estimates the strong collision rate constant for unimolecular decomposition of the adduct. The rate constant for the association reaction is obtained using the equilibrium constant. The thermochemical parameters used in the calculation are given in Table 13. HOOOCl frequencies are from Table 8 and structural parameters are from Table 7. The A, B and C rotational constants corresponding to these parameters are 18.0264148 GHz, 3.4782429 GHz and 3.1368345 GHz, respectively.

The results of the calculations are shown in Figure 8 which gives the strong collision association rate constant, $k_{rec,sc}^{HOOOCl}$, as a function of the HOOOCl enthalpy of formation at 200 K and 300 K. Also shown in the figure are the uncertainty limits associated with a ± 10% variation in the HOOOCl vibrational frequencies. $k_{rec,sc}^{HOOOCl}$ is a sensitive function of $\Delta H_f^o(0K)$, ranging from (2-70)x10^{-33} cm^6 molecule^{-2} s^{-1} at 300 K and (4-200)x10^{-33} cm^6 molecule^{-2} s^{-1} at 200 K over the assumed uncertainty range in $\Delta H_f^o(0K)$. The 10% uncertainty in vibrational frequencies results in about a factor of 3 uncertainty in $k_{rec,sc}^{HOOOCl}$.

At the upper limit of these estimates, the reaction to form HOOOCl would influence the measurement of the overall rate constant for the HO_2 + ClO reaction at high pressures. At 50 Torr, assuming that the reaction is in the low-pressure limiting regime, the recombination would enhance the observed rate of reactant disappearance by about 10%. Assuming no falloff the association channel would nearly double the rate at 700 Torr although significant falloff is expected at this pressure. These estimates are not corrected for weak collisions. Since significant pressure dependence was not observed in this study between 50-700 Torr, $k_{rec,sc}^{HOOOCl}$ must be smaller than about 1x10^{-31} cm^6 molecule^{-2} s^{-1}. If HOOOCl were to form, it would either accumulate as a stable product or react with another species in the system. Finkbeiner *et al.*[35] searched for IR absorption bands attributable to $HClO_3$ isomers in their static-photolysis/matrix-FTIR experiment using the *ab initio* band positions of Buttar and Hirst[12] but were unable to

obtain any evidence of complex formation. Apart from low inherent stability of the complexes, there are a number of possible explanations for this including insufficient instrumental sensitivity or band strength of the isomers, errors in the predicted band positions, and secondary reactions which remove the isomers including photolysis and the reaction with ClO or other radicals in the system.

Conclusions

The results presented here lead to a significantly different rate expression for the temperature dependence of the ClO + HO_2 rate constant than the results of Stimpfle *et al.* In contrast to the previous work, the reaction displayed linear Arrhenius behavior over the entire temperature range with a temperature dependence that is smaller than earlier measurements. This is also supported by recent discharge-flow results from our laboratory.

The existing database on the temperature dependence of k_1 does not reveal a consistent pattern. The two studies from our laboratory obtain a temperature dependence that is smaller than that measured by Stimpfle *et al.* but the flash photolysis results from the present study are consistently larger than the discharge-flow results. The resulting spread in the measured rate constants at temperatures relevant to the lower stratosphere (200-220 K) is a factor of 3 – 4. This has significant implications for the ability of atmospheric models to predict the rate of the important ClO + HO_2 catalytic ozone destruction cycle. It will also affect the comparison between atmospheric measurements of HOCl and model calculations[43].

New *ab initio* calculations on the energetics of $HClO_3$ intermediates and their transition states show that the formation of HOOOCl and HOOClO is energetically favorable, however there are large barriers on the singlet potential energy surface for formation of products from these intermediates. The termolecular formation rate of HOOOCl is sensitive to the calculated well depth and is therefore somewhat uncertain. The primary reactive pathway probably occurs on the triplet surface through a weakly bound hydrogen-bonded intermediate.

If HOOOCl is formed in the lower stratosphere and possesses an absorption band in the near-ultraviolet, it will photolyze to give HO_2 + ClO and OH + ClOO. The first channel is a null cycle with respect to ozone loss but the second channel is equivalent to the catalytic cycle involving ClO + HO_2 reaction on the triple surface. If photolysis of HOOOCl is slow then it may react with other radicals such as Cl, ClO or OH.

Acknowledgements

We would like to acknowledge the expert technical assistance of Mr. Dave Natzic in the setup and execution of these experiments. We have benefited greatly from frequent discussions with Dr. M. Okumura (Caltech), Dr. R. Salawitch and members of the JPL Chemical Kinetics and Photochemistry Group. Support for L. Blakeley was provided under an NIH Minority Access to Research Careers (MARC) Grant, no. GM08228. The supercomputer used in this investigation was provided by funding from the NASA Offices of Earth Science, Aeronautics and Space Science. The research was carried out by the Jet Propulsion Laboratory, California Institute of Technology, under contract with the National Aeronautics and Space Administration.

References

(1) WMO *Scientific Assessment of Ozone Depletion: 1998*; World Meteorological Association: Geneva, 1999.

(2) Salawitch, R.; McElroy, M. *Science* **1989**, *243*, 763-770.

(3) Lary, D. J. *J. Geophys. Res.* **1997**, *102*, 21515-21526.

(4) Li, Z.; Friedl, R. R.; Sander, S. P. *J. Phys. Chem.* **1995**, *99*, 13445-13451.

(5) Sander, S. P.; Friedl, R. R. *J. Phys. Chem.* **1989**, *93*, 4764-4771.

(6) Friedl, R. R.; Sander, S. P. *J. Phys. Chem.* **1989**, *93*, 4756-4764.

(7) Stimpfle, R.; Perry, R.; Howard, C. J. *J. Chem. Phys.* **1979**, *71*, 5183-5190.

(8) Mozurkewich, M. *J. Phys. Chem.* **1986**, *90*, 2216.

(9) Toohey, D. W.; Anderson, J. G. *J. Phys. Chem.* **1989**, *93*, 1049.

(10) McGrath, M. P.; Clemitshaw, K. C.; Rowland, F. S.; Hehre, W. J. *J. Phys. Chem.* **1990**, *94*, 6126.

(11) Colussi, A. J.; Grela, M. A. *J. Phys. Chem.* **1993**, *97*, 3775.

(12) Buttar, D.; Hirst, D. M. *J. Chem. Soc. Faraday Trans.* **1994**, *90*, 1811.

(13) Rohlfing, C. M. *Chem. Phys. Lett.* **1995**, *245*, 665-670.

(14) Phillips, D. H.; Quelch, G. E. *J. Phys. Chem.* **1996**, *100*, 11270-11275.

(15) Francisco, J. S.; Sander, S. P. *J. Phys. Chem* **1996**, *100*, 573-579.

(16) Nickolaisen, S. L.; Friedl, R. R.; Sander, S. P. *J. Phys. Chem.* **1994**, *98*, 155-169.

(17) DeMore, W. B.; Sander, S. P.; Golden, D. M.; Hampson, R. F.; Kurylo, M. J.; Howard, C. J.; Ravishankara, A. R.; Kolb, C. E.; Molina, M. J. Chemical Kinetics and Photochemical Data for Use in Stratospheric Modeling. In *JPL Publication 97-4*; Jet Propulsion Laboratory, Calif. Inst. of Technology: Pasadena, CA, 1997.

(18) Nickolaisen, S.; Miller, C.; Sander, S.; Hand, M.; Williams, I.; Francisco, J. *J. Chem. Phys.* **1996**, *104*, 2857-2868.

(19) Tanaka, Y.; Kawasaki, M.; Matsumi, Y.; Fujiwara, H.; Ishiwata, T.; Rogers, L.; Dixon, R.; Ashfold, M. *J. Chem. Phys.* **1998**, *109*, 1315-1323.

(20) Moore, T.; Okumura, M.; Minton, T. *J. Chem. Phys.* **1997**, *107*, 3337-3338.

(21) Cady, G. H. *Inorg. Syn.* **1967**, *5*, 156.

(22) Frisch, M. J.; Trucks, G. W.; Head-Gordon, M.; Gill, P. M. W.; Wong, M. W.; Foresman, J. B.; Johnson, B. G.; Schlegel, H. B.; Robb, M. A.; Replogle, E. S.; Gomperts, R.; Andres, J. L.; Raghavachari, K.; Binkley, J. S.; Gonzalez, C.; Martin, R. J.; Fox, D. J.; Defrees, B. J.; Baker, J.; Stewart, J. J. P.; Pople, J. A. GAUSSIAN 94; Gaussian, Inc.: Pittsburgh, PA, 1994.

(23) Becke, A. D. *J. Chem. Phys.* **1993**, *98*, 1372.

(24) Lee, C.; Yang, W.; Parr, R. G. *Phys. Rev.* **1988**, *B41*, 785.

(25) Lee, T. J.; Rendell, A. P. *J. Chem. Phys.* **1991**, *94*, 6219.

(26) Curtis, A. R.; Sweetenham, W. P. FACSIMILE/CHEKMAT; H015 ed.; Harwell: Oxfordshire, 1987.

(27) Maricq, M. M.; Szente, J. J. *J. Phys. Chem.* **1994**, *98*, 2078-2082.

(28) Simon, F. G.; Schneider, W.; Moortgat, G. K.; Burrows, J. P. *J. Photochem. Photobiol.* **1990**, *A55*, 1-23.

(29) Reimann, B.; Kaufman, F. *J. Chem. Phys.* **1978**, *69*, 2925 .

(30) Leck, T. J.; Cook, J. E.; Birks, J. W. *J. Chem. Phys.* **1980**, *72*, 2364-2373.

(31) Cattell, F. C.; Cox, R. A. *J. Chem. Soc. Faraday Trans. 2* **1986**, *82*, 1413-1426.

(32) Burrows, J. P.; Cox, R. A.; Derwent, R. G. *J. Photochem.* **1981**, *16*, 147-168.

(33) Atkinson, R.; Baulch, D. L.; Cox, R. A.; Hampson, R. F.; Kerr, J. A.; Troe, J. *J. Phys. Chem. Ref. Data* **1992**, *21*, 1125-1568.

(34) Laszlo, B.; Friedl, R. R.; Sander, S. P. *to be submitted to J. Phys. Chem.* **1999**.

(35) Finkbeiner, M.; Crowley, J. N.; Horie, O.; Muller, R.; Moortgat, G. K.; Crutzen, P. J. *J. Phys. Chem.* **1995**, *99*, 16264-16275.

(36) Leu, M. T. *Geophys. Res. Lett.* **1980**, *7*, 173-175.

(37) Burrows, J. P.; Cox, R. A. *J. Chem. Soc. Faraday Trans. 1* **1981**, *77*, 2465.

(38) Toohey, D. W.; Anderson, J. G. *J. Phys. Chem.* **1988**, *92*, 1705-1708.

(39) Grela, M.; Colussi, A. J. *J. Phys. Chem.* **1996**, *100*, 10150.

(40) Troe, J. *J. Chem. Phys.* **1977**, *66*, 4745 .

(41) Troe, J. *J. Chem. Phys.* **1977**, *66*, 4758.

(42) Patrick, R.; Golden, D. M. *Int. J. Chem. Kinet.* **1983**, *15*, 1189-1227.

(43) Salawitch, R. J. *to be submitted* .

(44) Steunenberg, R. K.; Vogel, R. C. *J. Am. Chem. Soc.* **1956**, *78*, 901-902.

Table 1. Concentration ranges of precursor and radical species for ClO + HO_2 kinetic measurements.

$F_2/Cl_2O/H_2/O_2$ system	
Species	Concentration Range (molecule cm^{-3})
$[F_2]_o$	$(1.5 - 7.0) \times 10^{16}$
$[Cl_2O]_o$	$(8.0 - 20) \times 10^{12}$
$[O_2]_o$	$(3.0 - 4.5) \times 10^{17}$
$[H_2]_o$	$(3.5 - 4.5) \times 10^{17}$
$[ClO]_o$	$(2.8 - 53) \times 10^{12}$
$[HO_2]_o$	$(1.6 - 15) \times 10^{13}$

$Cl_2/CH_3OH/Cl_2O/O_2$ system	
Species	Concentration Range (molecule cm^{-3})
$[CH_3OH]_o$	$(1.5 - 30) \times 10^{14}$
$[Cl_2O]_o$	$(1.4 - 3.5) \times 10^{14}$
$[Cl_2]_o$	$(2.0 - 3.0) \times 10^{16}$
$[O_2]_o$	$(5.5 - 7.5) \times 10^{17}$
$[ClO]_o$	$(9.3 - 80) \times 10^{12}$
$[HO_2]_o$	$(4.9 - 12) \times 10^{13}$

Table 2. 210 nm absorption cross sections at 298 K used in the kinetic analysis by FACSIMILE.

Species	Cross Section cm^2 $molecule^{-1}$	Reference
HO_2	$3.91x10^{-18}$	Mariq *et al.*[27]
ClO	$2.2x10^{-19}$	DeMore *et al.*[17]
Cl_2O_2	$2.51x10^{-18}$	DeMore *et al.*[17]
H_2O_2	$3.57x10^{-19}$	DeMore *et al.*[17]
HOCl	$5.7x10^{-20}$	DeMore *et al.*[17]
Cl_2O	$2.38x10^{-19}$	DeMore *et al.*[17]
F_2	$4.2x10^{-21}$	Steunenberg and Vogel[44]

Table 3. Reaction mechanism used in analysis of data obtained using the $F_2/Cl_2O/H_2/O_2$ source chemistry.

Reaction	Rate coefficient[1]
$ClO + HO_2 \rightarrow HOCl + O_2$	k_1
$HO_2 + HO_2 \rightarrow H_2O_2 + O_2$	k_2
$F + H_2 \rightarrow HF + H$	$1.4 \times 10^{-10} \exp(-500/T)$
$F + O_2 + M \rightarrow FO_2 + M$	$4.4 \times 10^{-33} (T/300)^{-1.2}$
$H + O_2 + M \rightarrow HO_2 + M$	$5.7 \times 10^{-32} (T/300)^{-1.6}$
$HO_2 + HO_2 + M \rightarrow H_2O_2 + M$	$1.7 \times 10^{-33} \exp\{1000/T\}$
$Cl + Cl_2O \rightarrow ClO + Cl_2$	$6.2 \times 10^{-11} \exp\{130/T\}$
$Cl + HO_2 \rightarrow HCl + O_2$	$1.8 \times 10^{-11} \exp\{170/T\}$
$Cl + HO_2 \rightarrow ClO + OH$	$4.1 \times 10^{-11} \exp\{-450/T\}$
$F + HO_2 \rightarrow HF + O_2$	8.3×10^{-11}
$F + Cl_2O \rightarrow ClF + ClO$	$1.5 \times 10^{-10} \exp\{-47/T\}$
$H + HO_2 \rightarrow 2\ OH$	$2.8 \times 10^{-10} \exp\{-440/T\}$
$ClO + ClO + M \rightarrow Cl_2O_2 + M$[2]	k_o: $2.2 \times 10^{-32} (T/300)^{-3.1}$
	k_∞: $3.5 \times 10^{-12} (T/300)^{-1.0}$
$Cl_2O_2 + M \rightarrow ClO + ClO + M$	$K_{eq} = 1.3 \times 10^{-27} \exp\{8744/T\}$
$ClO + ClO \rightarrow Cl_2 + O_2$	$1.0 \times 10^{-12} \exp\{-1590/T\}$
$ClO + ClO \rightarrow 2\ Cl + O_2$	$3.0 \times 10^{-11} \exp\{-2450/T\}$
$ClO + ClO \rightarrow OClO + Cl$	$3.5 \times 10^{-13} \exp\{-1370/T\}$
$Cl + OClO \rightarrow 2\ ClO$	$3.4 \times 10^{-11} \exp\{160/T\}$

[1]Units for bimolecular reactions are cm^3 $molecule^{-1}$ s^{-1}.
Units for termolecular reactions are cm^6 $molecule^{-2}$ s^{-1}
Rate coefficients are from DeMore *et al.*[17]
[2]Rate constants for ClO + ClO + M reaction are calculated from

$$k_f(M,T) = \left(\frac{k_o(T)[M]}{1 + \left(\frac{k_o(T)[M]}{k_\infty(T)} \right)} \right) 0.6^{\left\{ 1 + \left[\log_{10}\left(\frac{k_o(T)[M]}{k_\infty[T]} \right)^2 \right] \right\}^{-1}}$$

Table 4. Reaction mechanism used in analysis of data using the $Cl_2/Cl_2O/CH_3OH/O_2$ reactant source chemistry.

Reaction	Rate coefficient[1]
$ClO + HO_2 \rightarrow HOCl + O_2$	k_1
$HO_2 + HO_2 \rightarrow H_2O_2 + O_2$	k_2
$Cl + Cl_2O \rightarrow ClO + Cl_2$	k_3
$Cl + CH_3OH \rightarrow CH_2OH + HCl$	5.4×10^{-11}
$CH_2OH + O_2 \rightarrow HO_2 + CH_2O$	9.1×10^{-12}
$HO_2 + HO_2 + M \rightarrow H_2O_2 + M$	$1.7 \times 10^{-33} \exp\{1000/T\}$
$Cl + HO_2 \rightarrow HCl + O_2$	$1.8 \times 10^{-11} \exp\{170/T\}$
$Cl + HO_2 \rightarrow ClO + OH$	$4.1 \times 10^{-11} \exp\{-450/T\}$
$Cl + CH_2O \rightarrow HCl + HCO$	$8.1 \times 10^{-11} \exp\{-30/T\}$
$HCO + O_2 \rightarrow CO + HO_2$	$3.5 \times 10^{-12} \exp\{140/T\}$
$HCO + Cl_2 \rightarrow HCOCl + Cl$	$6.1 \times 10^{-12} \exp\{-36/T\}$
$ClO + ClO + M \rightarrow Cl_2O_2 + M$[2]	k_o: $2.2 \times 10^{-32} (T/300)^{-3.1}$
	k_∞: $3.5 \times 10^{-12} (T/300)^{-1.0}$
$Cl_2O_2 + M \rightarrow ClO + ClO + M$	$K_{eq} = 1.3 \times 10^{-27} \exp\{8744/T\}$
$ClO + ClO \rightarrow Cl_2 + O_2$	$1.0 \times 10^{-12} \exp\{-1590/T\}$
$ClO + ClO \rightarrow 2\,Cl + O_2$	$3.0 \times 10^{-11} \exp\{-2450/T\}$
$ClO + ClO \rightarrow OClO + Cl$	$3.5 \times 10^{-13} \exp\{-1370/T\}$
$Cl + Cl_2O_2 \rightarrow Cl + Cl_2 + O_2$	1.0×10^{-10}
$Cl + OClO \rightarrow 2\,ClO$	$3.4 \times 10^{-11} \exp\{160/T\}$

[1]Units for bimolecular reactions are cm^3 $molecule^{-1}$ s^{-1}.
Units for termolecular reactions are cm^6 $molecule^{-2}$ s^{-1}
Rate coefficients are from DeMore *et al.*[17]
[2]Rate constants for ClO + ClO + M reaction are calculated from

$$k_f(M,T) = \left(\frac{k_o(T)[M]}{1 + \left(\frac{k_o(T)[M]}{k_\infty(T)} \right)} \right) 0.6^{\left\{ 1 + \left[\log_{10}\left(\frac{k_o(T)[M]}{k_\infty[T]} \right)^2 \right] \right\}^{-1}}$$

Table 5. Summary of rate coefficient data, uncertainties, and number of measurements performed for each chemical system at specified experimental temperatures.

Temp. (K)	Source Chemistry[1]	k (10^{-12} cm^3 molecule^{-1} s^{-1})	$[ClO]_o$ (10^{13} molecule cm^{-3})	$[HO_2]_o$ (10^{13} molecule cm^{-3})	$\frac{[ClO]_o}{[HO_2]_o}$	No. of experiments
203	F_2	12.15 ± 2.20	0.6 – 5.3	2.4 – 10.1	0.06 – 1.45	13
215	Cl_2	10.60 ± 1.49	2.3 – 8.0	4.5 – 12.2	0.22 – 1.67	10
	F_2	13.62 ± 1.62	2.1 – 2.8	6.7 – 12.7	0.22 – 0.34	5
221	F_2	13.67 ± 1.49	1.3 – 1.4	3.5 – 7.1	0.18 – 0.40	5
228	Cl_2	10.95 ± 1.43	1.9 – 5.7	6.5 – 10.6	0.17 – 0.83	15
	F_2	12.13 ± 1.43	1.1 – 2.9	2.2 – 12.0	0.24 – 0.59	10
240	Cl_2	9.35 ± 1.25	1.1 – 4.5	6.2 – 11.0	0.10 – 0.67	15
	F_2	10.93 ± 1.38	0.63 – 1.3	3.0 – 8.9	0.11 – 0.42	15
252	F_2	10.37 ± 1.20	1.3 – 1.4	3.5 – 8.7	0.16 – 0.39	5
265	Cl_2	8.65 ± 1.05	1.3 – 5.4	5.1 – 10.0	0.14 – 1.07	15
	F_2	9.11 ± 1.30	0.5 – 3.3	1.6 – 9.7	0.12 – 0.70	23
277	Cl_2	8.16 ± 0.95	1.3 – 8.0	5.4 – 12.3	0.11 – 1.48	10
285	F_2	9.08 ± 1.35	0.4 – 1.2	2.8 – 5.5	0.08 – 0.29	9
299	Cl_2	7.78 ± 0.83	1.5 – 3.9	7.9 – 12.1	0.12 – 0.50	15
	F_2	8.26 ± 1.38	0.67 – 5.0	1.6 – 7.3	0.12 – 0.94	25
314	Cl_2	7.34 ± 0.82	1.5 – 4.6	8.2 – 11.7	0.14 – 0.55	13
	F_2	7.89 ± 1.16	1.2 – 3.3	5.0 – 15.0	0.17 – 0.36	15
339	Cl_2	6.82 ± 0.82	1.0 – 5.9	5.9 – 11.6	0.13 – 0.97	15
	F_2	7.55 ± 1.03	1.3 – 2.3	4.6 – 14.1	0.14 – 0.39	15
364	Cl_2	6.55 ± 0.74	0.93 – 9.6	2.0 – 9.0	0.12 – 4.85	15
	F_2	7.06 ± 0.90	0.80 – 2.4	4.1 – 10.8	0.17 – 0.38	15

[1] F_2 denotes F_2-H_2-O_2-Cl_2O system, Cl_2 denotes Cl_2-Cl_2O-CH_3OH-O_2 system

Table 6. Sensitivity of fitted value of k_1 to uncertainties in other parameters used in least-squares fitting routine reported as a percent change.

Parameter	Uncertainty[1]	Sensitivity (% change)
$k_{ClO+ClO+M}$	+15%/-25%[2]	+0.27/-0.23 %
$k_{Cl2O2+M}$	B = ± 850[3]	+1.38/-0.27 %
σ_{HO2}	± 10%	+9.21/-8.65 %
σ_{ClO} (275 nm)	± 10%	+0.89/-1.01 %
σ_{ClO} (210 nm)	± 20%	+0.30/-0.27 %
σ_{H2O2}	± 30%	+1.49/-0.59 %
σ_{Cl2O2}	± 50%	+0.09/-0.06 %
σ_{HOCl}	± 40%	+0.25/-0.17 %
σ_{Cl2O}	± 10%	-0.39/+0.37 %

[1]Taken from the assessment of DeMore *et al.*[17]

[2]The percentages represent the maximum change when varying k_o, k_∞, m and n by their stated uncertainties in the falloff expression used by DeMore *et al.*[17]

[3]The value of the B parameter in the expression for the equilibrium constant given in DeMore *et al.* was varied by its stated uncertainties.

Table 7. Geometries of reactants, intermediates, and transition states in the HO_2 + ClO reaction[a]

Species	Parameter	B3LYP/6-311++G(3df,3pd)
Reactants and Products		
ClO	ClO	1.576
$O_2(^1\Delta)$	OO	1.203
$O_2(^1\Sigma g)$	OO	1.203
HCl	HCl	1.281
HOCl	HO	0.966
	ClO	1.700
	HOCl	103.7
HO_2	HO	0.975
	OO	1.324
	HOO	105.5
O_3	OO	1.251
	OOO	118.3
HOOClO′	HO	0.969
	OO	1.422
	ClO	1.503
	ClO′	1.750
	HOO	102.2
	OOCl	111.2
	OClO′	113.6
	HOOCl	92.2
	OOClO′	80.1
HOOO′Cl	HO	0.970
	OO	1.423
	OO′	1.387
	O′Cl	1.740
	HOO	102.1
	OOO′	108.8
	OO′Cl	111.2
	HOOO′	77.9
	OOO′Cl	82.5

Transition States		
$HOOClO \rightarrow HOCl+O_2(^1\Delta)$	HO′	1.581
	HO	1.027
	OO	1.306
	ClO	2.282
	ClO′	1.609
	HOO	105.1
	OOCl	94.3
	OClO′	85.1
	OHO′	121.9
	ClO′H	100.2
	HOOCl	44.3
	OOClO′	-15.4
$HOOOCl \rightarrow HOCl+O_2(^1\Delta)$	HO	1.029
	OO	1.288
	OO′	2.236
	O′Cl	1.649
	HO′	1.572
	HOO	100.4
	OOO′	71.3
	OO′Cl	151.2
	OO′H	52.6
	HOOO′	-32.5
	OOO′Cl	71.3
$HOOOCl \rightarrow HCl+O_3$	HO	1.193
	OO	1.354
	OO′	1.254
	O′Cl	2.568
	HCl	1.593
	HOO	98.1
	OOO′	111.8
	OO′Cl	94.9
	O′ClH	55.6
	HOOO′	-37.3
	OOO′Cl	44.8

[a]Bond distances in Å and bond angles in degrees.

Table 8. Calculated vibrational frequencies and zero-point energies of the species in the HO_2+ClO reaction

Species	Frequencies (cm^{-1})[a]	Zero-point energies (kcal mol^{-1})[a]
Reactants and Products		
ClO	833	1.2
HO_2	3581, 1429, 1176	8.9
HCl	2958	4.2
HOCl	3761, 1273, 723	8.2
$O_2(^1\Delta)$	1643	2.3
$O_2(^3\Sigma g)$	1658	2.4
O_3	1266, 1241, 735	4.6
HOOClO	3693, 1408, 964, 922, 479, 449, 317, 214, 110	12.1
HOOOCl	3703, 1404, 918, 722, 597, 531, 416, 301, 154	12.6
Transition States		
HOOClO → HOCl+$O_2(^1\Delta)$	2865, 1543, 1217, 842, 484, 403, 27 185, 428i	11.2
HOOOCl → HOCl+$O_2(^1\Delta)$	2820, 1453, 1248, 792, 532, 313, 277, 83, 395i	10.7
HOOOCl → HCl+O_3	1539, 1257, 1051, 884, 734, 450, 365, 200, 1106i	9.3

[a]Calculated at the B3LYP/6-31G(d,p) level of theory.

Table 9. Relative Energies on the Triplet Surface for the HO_2 + ClO Reaction for Reactants, Products, Complex and Transition State.

Theory/Basis Set	$HO_2 + ClO \rightarrow ClO^{\cdots}HO_2$	$HO_2 + ClO \rightarrow [ClO^{\cdots}HO_2]^{\ddagger}$		$HO_2 + ClO \rightarrow HOCl + O_2$
	Complex	*Cis*	*Trans*	
UMP2/6-31G(d)	-2.5	2.2	5.1	-64.1
CCSD(T)/6-31G(d)	-3.0	-0.9	2.3	-47.8
CCSD(T)/6-311G(d,p)	-2.7	-1.8	-0.2	-50.2
CCSD(T)/6-311G(2d,2p)	-3.1	-2.8	0.3	-48.9
CCSD(T)/6-311++G(2df,2p)	-2.8	-2.4	0.7	-47.1
Expt.				-45.5

Table 10. Total energies (in hartrees) of the species in the HO_2 + ClO reaction

Species	B3LYP 6-311++G(3df,3pd)	CCSD(T)[a] 6-311++G(3df,3pd)
Reactants and Products		
ClO	-535.36509	-534.72879
HO_2	-150.96833	-150.71339
HCl	-460.83904	-460.33066
$O_2(^1\Delta)$	-150.31815	-150.08002
$O_2(^3\Sigma g)$	-150.37948	-150.12825
O_3	-225.49798	-225.13259
HOCl	-536.02204	-535.38893
HOOClO	-686.33089	-685.44542
HOOOCl	-686.35353	-685.47076
Transition States		
HOOClO $\rightarrow$ HOCl+$O_2(^1\Delta)$	-686.32061	-685.43718
HOOOCl $\rightarrow$ HOCl+$O_2(^1\Delta)$	-686.29479	-685.42872
HOOOCl $\rightarrow$ HCl+O_3	-686.31358	-685.42935

[a]Calculated using the geometries of the B3LYP/6-311++G(3df,3pd) level of theory.

Table 11. Relative energies (in kcal mol^{-1}) for reaction pathways in the HO_2 + ClO reaction

	6-311++G(3df,3pd)		
Reaction	**B3LYP**	**CCSD(T)**	**Expt.**
$HO_2+ClO \rightarrow HOCl+O_2(^3\Sigma g)$	-42.1	-46.6	-45.6
$HO_2+ClO \rightarrow HOCl+O_2(^1\Delta)$	-3.8	-16.4	
$HO_2+ClO \rightarrow HCl+O_3$	-3.6	-14.5	-15.8
$HO_2+ClO \rightarrow HOOClO$	3.6	-0.02	
$HO_2+ClO \rightarrow HOOOCl$	-10.1	-15.4	
$HOOClO \rightarrow HOCl+O_2(^1\Delta)$	-7.4	-16.4	
$HOOClO \rightarrow [HOCl+O_2(^1\Delta)]^{\ddagger}$	5.6	4.3	
$HOOOCl \rightarrow HOCl+O_2(^1\Delta)$	6.3	-1.0	
$HOOOCl \rightarrow [HOCl+O_2(^1\Delta)]^{\ddagger}$	35.0	24.5	
$HOOOCl \rightarrow HCl+O_3$	6.6	0.9	
$HOOOCl \rightarrow [HCl+O_3]^{\ddagger}$	21.8	22.7	

Table 12. Comparison of *ab initio* Calculations on HOOOCl Energetics

Reference	Method	Result quoted in ref., kcal mol^{-1}	ΔH°_{f}(298 K)* kcal mol^{-1}
Stimpfle *et al.* (1979)	Group Additivity	25 ΔH_f°(298 K)	25
Buttar and Hirst (1994)	MP2/6-31G**	-26.3 ΔH_r° (0 K?)	-0.1
Rohlfing (1995)	G2	9.3 ΔH_f°(298 K)	9.3
Phillips and Quelch (1996)	MC1	-18.2 ΔH_r° (298 K)	9.0
Phillips and Quelch (1996)	FVMC	-11.7 ΔH_r° (298 K)	15.5
Francisco and Sander (1996)	G2	9.1 ΔH_f°(298 K)	7.4
This Work	CCSD(T)/6-311++G(3df,3pd)	-15.4 ΔH_r°	10.8
This Work	B3LYP/6-311++G(3df,3pd)	-10.1 ΔH_r°	16.1

*Result calculated using JPL97 values of ΔH_f°(298 K) for HO_2 and ClO, JANAF values of (ΔH_f°(0 K)- ΔH_f°(298 K)) and (ΔH_f°(0 K)- ΔH_f°(298 K)) for HOOOCl from this work (1.7 kcal mole^{-1}).

Table 13. Parameters Used in Calculations of the Rate Constant for the Reaction HO_2 + ClO + M → HOOOCl + M

Species	$\Delta H^{\circ}_{f}(0K)$ kJ mole^{-1}	$\Delta H^{\circ}_{f}(300K)$ kJ mole^{-1}	$S^{\circ}(300K)$ J (mole K)$^{-1}$	Ref.
HO_2	13.39	10.46	229.0	42
ClO	101.3	101.22	226.74	42
HOOOCl	50.21	43.14	295.31	this work

Figure Captions

Figure 1. Schematic diagram of flash photolysis/ultraviolet absorption apparatus. The cw probe consists of a 150 W deuterium lamp and a 300 W xenon arc lamp combined with a dichroic beamsplitter. Both probes traced the same 720 cm optical path within the flash photolysis cell. A second dichroic beamsplitter at the exit separated the probes into a long-wavelength component for ClO detection and a short-wavelength component for HO_2 detection.

Figure 2. Absorption spectra of species involved in the HO_2 + ClO kinetics studies. Arrows denote the wavelengths used for the detection of HO_2 at 210 nm and ClO by differential absorption at 275 nm.

Figure 3. Example of time-resolved absorption signals for the F_2-H_2-O_2-Cl_2O system. (a): 210 nm absorption channel (HO_2). (b): Differential absorption signal from 275.2 nm and 276.4 nm channels (ClO). The solid lines are fits obtained using FACSIMILE as discussed in the text.

Figure 4. Arrhenius plot of temperature-dependence data for the ClO + HO_2 reaction. (•): This work. Data obtained using the F_2-H_2-O_2-Cl_2O system. (■): This work. Data obtained using Cl_2-CH_3OH-O_2-Cl_2O system. (—): Fit to the combined data from both chemical systems. (– • • –): Fit to the data of Stimpfle *et al.*[7] (– – –): Recommendation from JPL 97-4 Data Evaluation[17]. (– • – •): Data obtained using the discharge flow/mass spectrometry technique at 1 Torr from this laboratory [34].

Figure 5. Transition state structures for reaction pathways on the singlet surface of the HO_2 + ClO reaction. Structures are calculated at the B3LYP/6-311++(3df,3pd) level of theory. **(a):** Transition state for the pathway HOOClO → HOCl + $O_2(^1\Delta)$. **(b):** Transition state for the pathway HOOOCl → HOCl + $O_2(^1\Delta)$. **(c):** Transition state for the pathway HOOOCl → HCl + O_3.

Figure 6. Transition state structures for reaction pathways on the triplet surface of the HO_2 + ClO reaction. Two values are given for each bond length. The upper value is the result obtained at the UMP2/6-31G(d) level of theory while the lower value is obtained using the CCSD(T)/6-31G(d) level of theory. **(a):** triplet state complex. **(b):** *cis* transition state. **(c):** *trans* transition state.

Figure 7. Schematic diagram showing energy levels and reaction pathways for the HO_2 + ClO reaction along the singlet and triplet pathways. Numbers next to chemical symbols refer to the Figures showing the corresponding structures.

Figure 8. Rate constants for the reaction HO_2 + ClO + M → HOOOCl + M vs. $\Delta H_f^o(0K)$ for HOOOCl at 300 K (solid lines) and 200 K (dashed lines). At each temperature the uncertainty band associated with a ± 10% uncertainty in the HOOOCl vibrational frequencies is indicated.

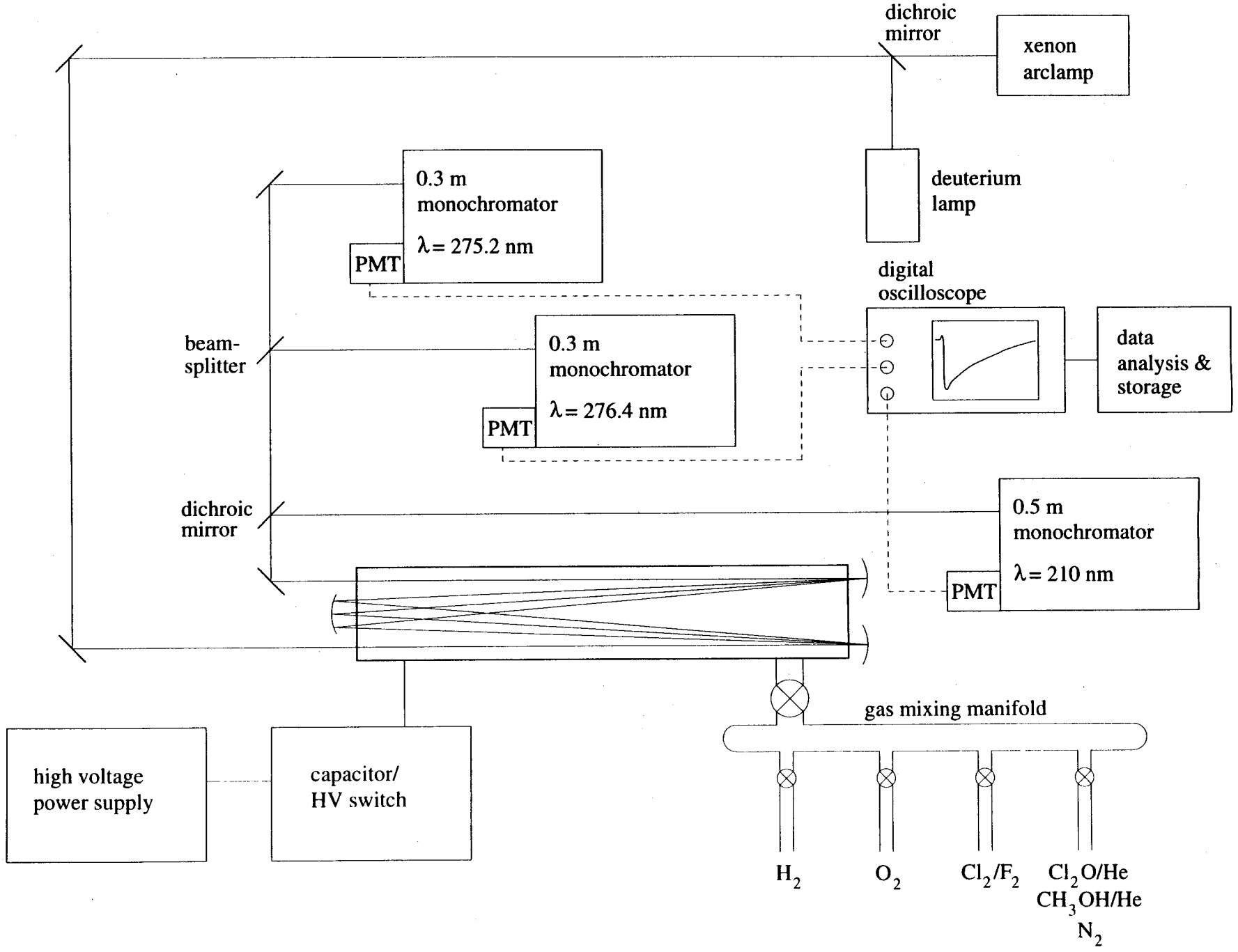
dichroic mirror
xenon arclamp
0.3 m monochromator
λ = 275.2 nm
PMT
deuterium lamp
digital oscilloscope
beam-splitter
0.3 m monochromator
λ = 276.4 nm
PMT
data analysis & storage
dichroic mirror
0.5 m monochromator
λ = 210 nm
PMT
gas mixing manifold
high voltage power supply
capacitor/ HV switch
H_2
O_2
Cl_2/F_2
Cl_2O/He
CH_3OH/He
N_2

Figure 1

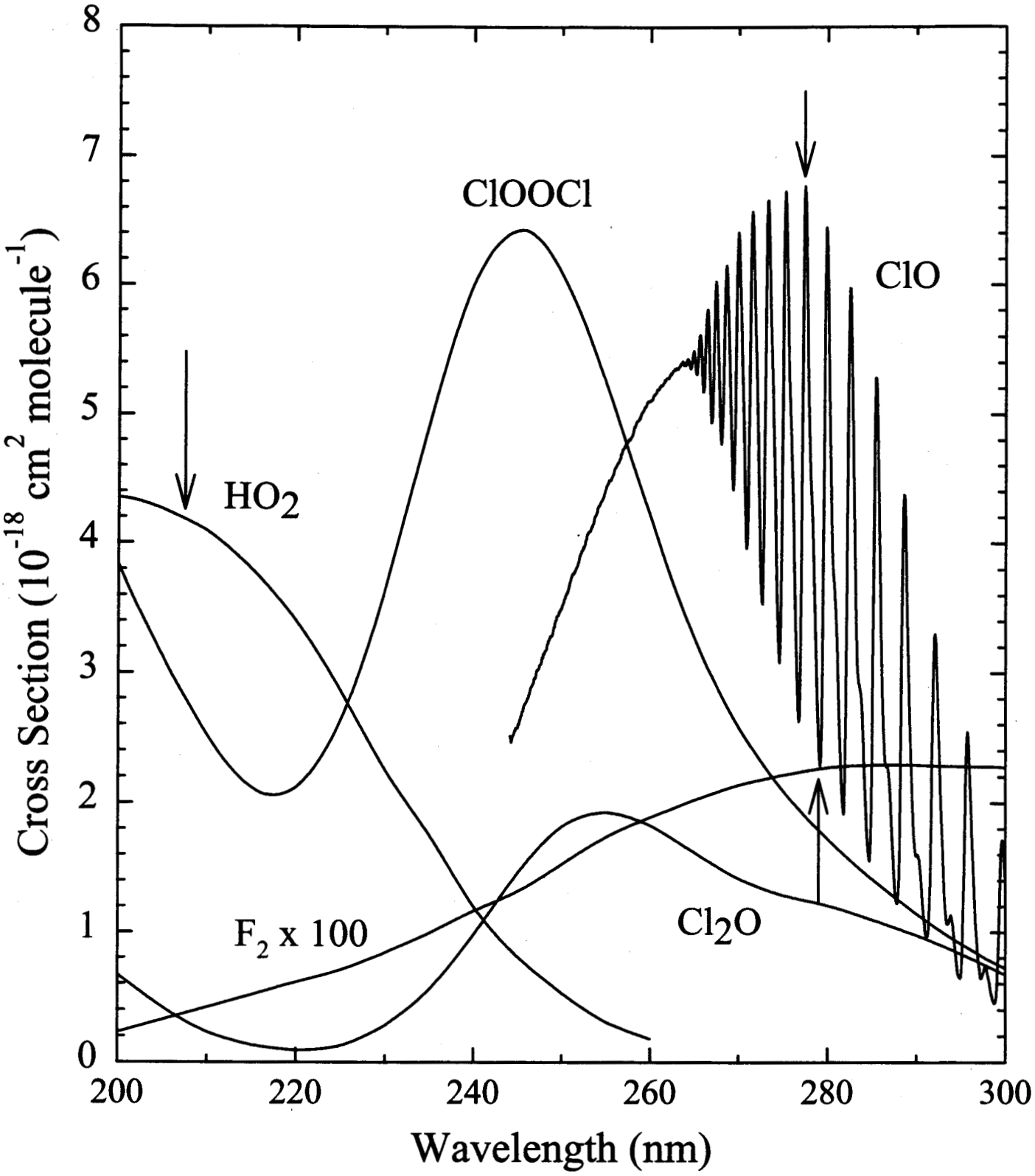
ClOOCl
ClO
HO2
F2 x 100
Cl2O
Cross Section (10-18 cm2 molecule-1)
Wavelength (nm)
0
1
2
3
4
5
6
7
8
200
220
240
260
280
300

Figure 2

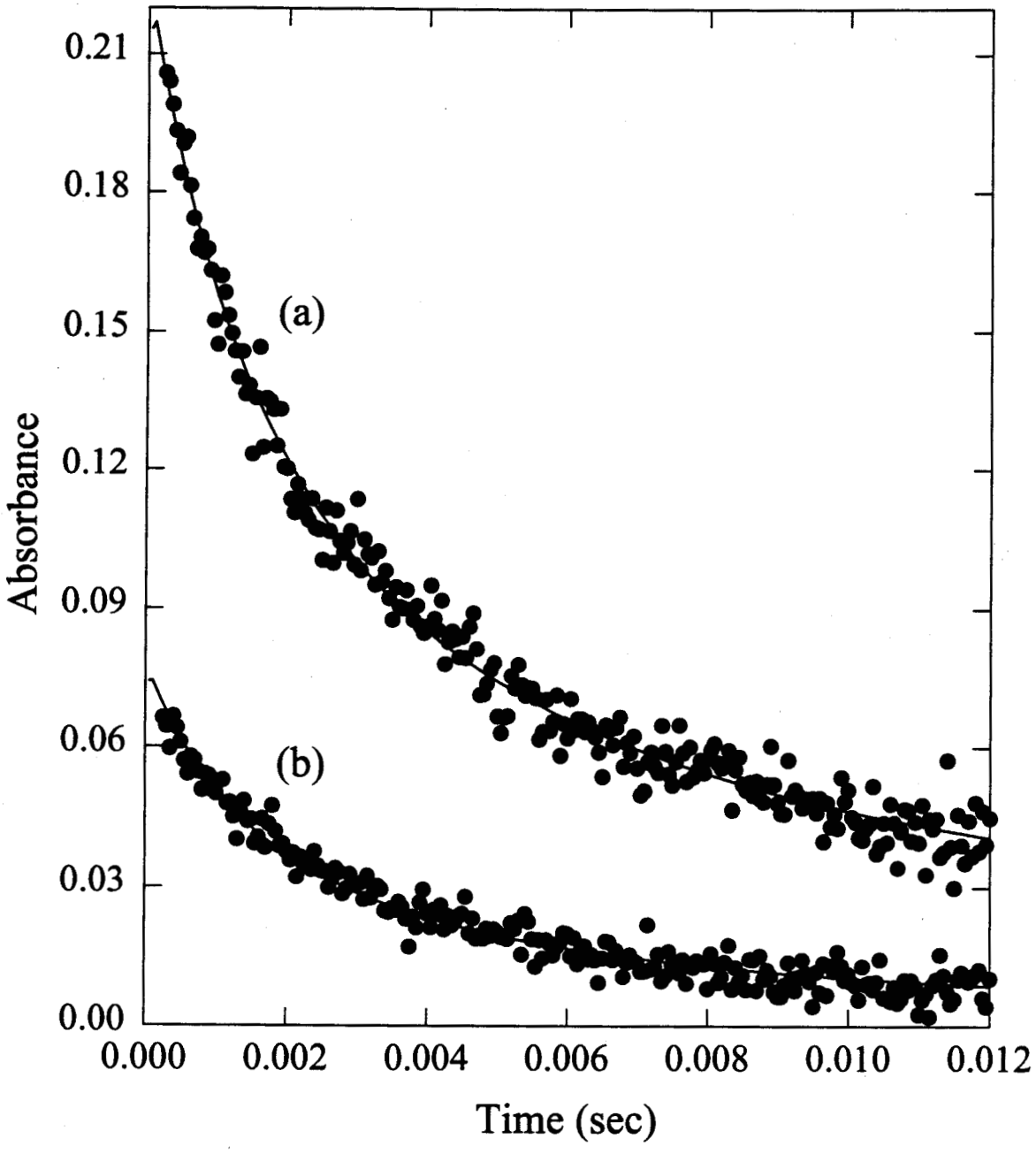
0.21
0.18
0.15
0.12
0.09
0.06
0.03
0.00
Absorbance
(a)
(b)
0.000
0.002
0.004
0.006
0.008
0.010
0.012
Time (sec)

Figure 3

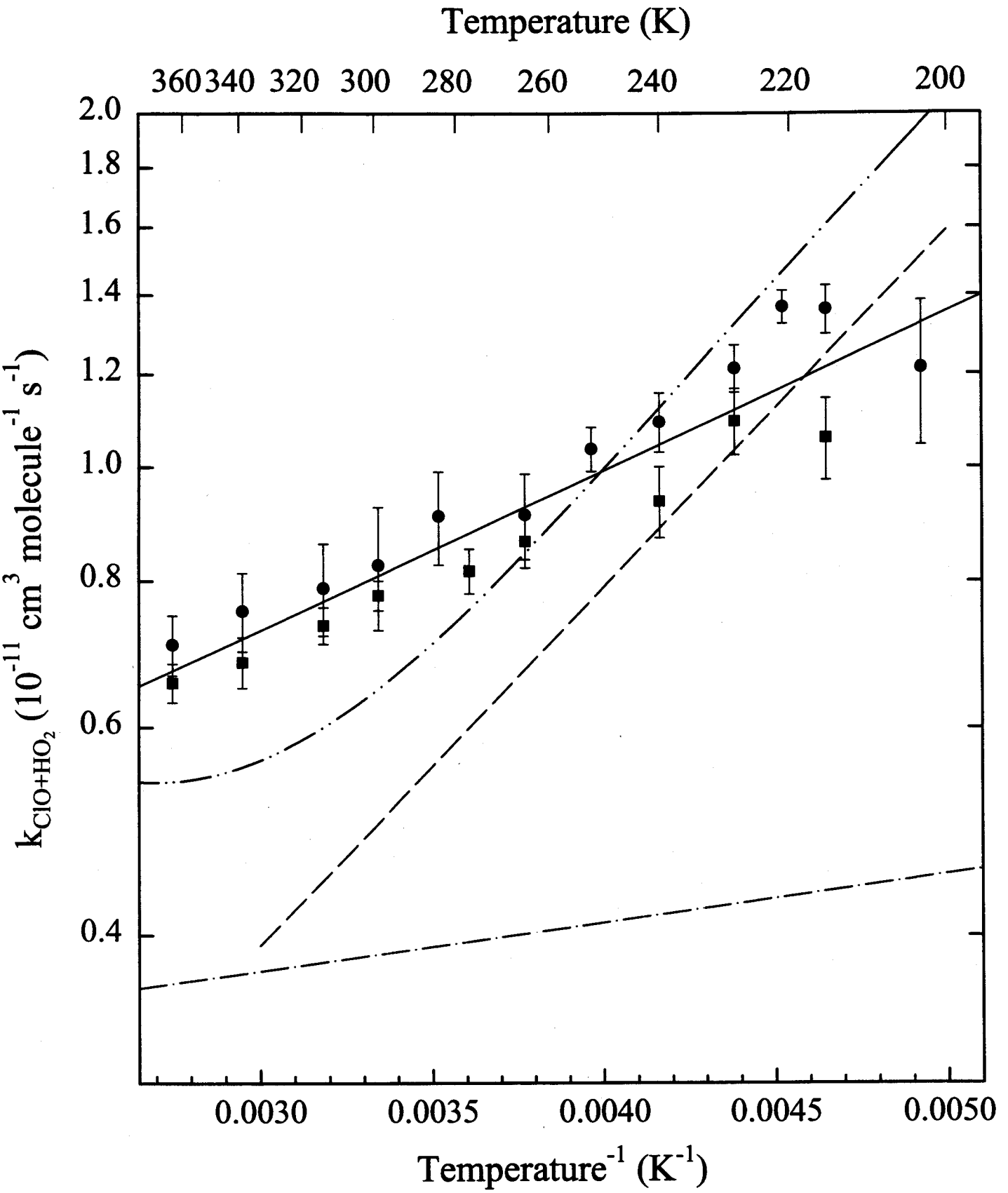
Temperature (K)
360 340 320 300 280 260 240 220 200
2.0
1.8
1.6
1.4
1.2
1.0
0.8
0.6
0.4
k_{ClO+HO_2} (10^{-11} cm^3 $molecule^{-1}$ s^{-1})
0.0030 0.0035 0.0040 0.0045 0.0050
Temperature^{-1} (K^{-1})

Figure 4

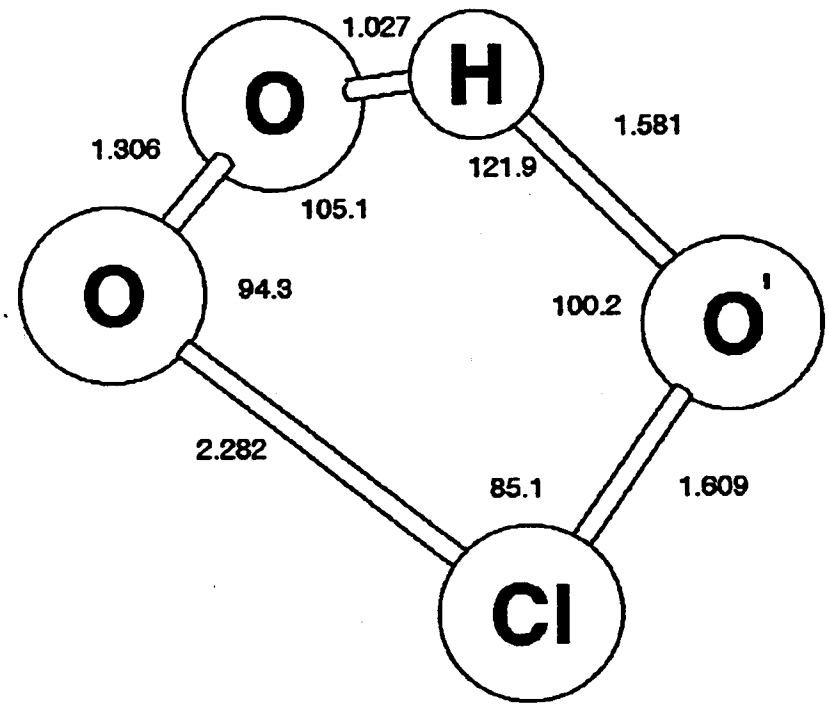

Figure 5a

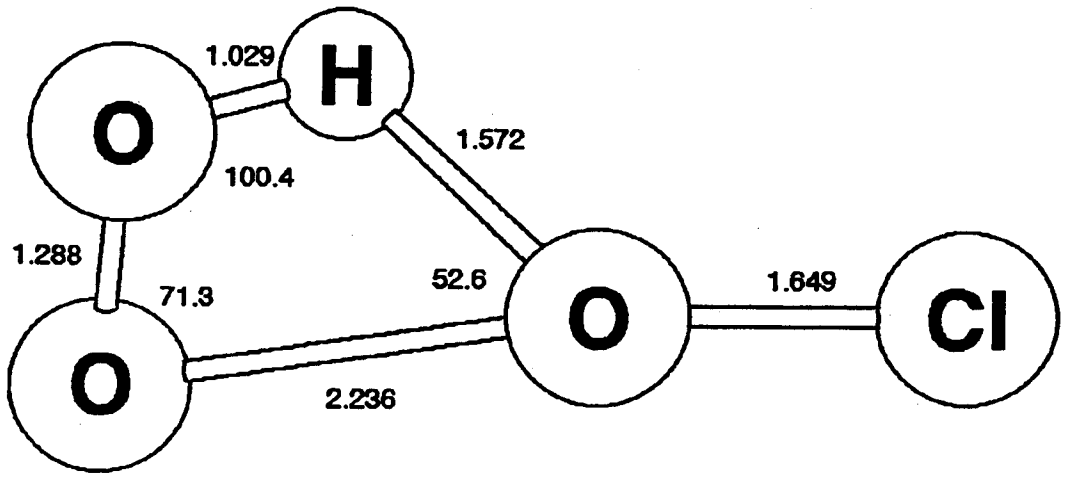

Figure 56

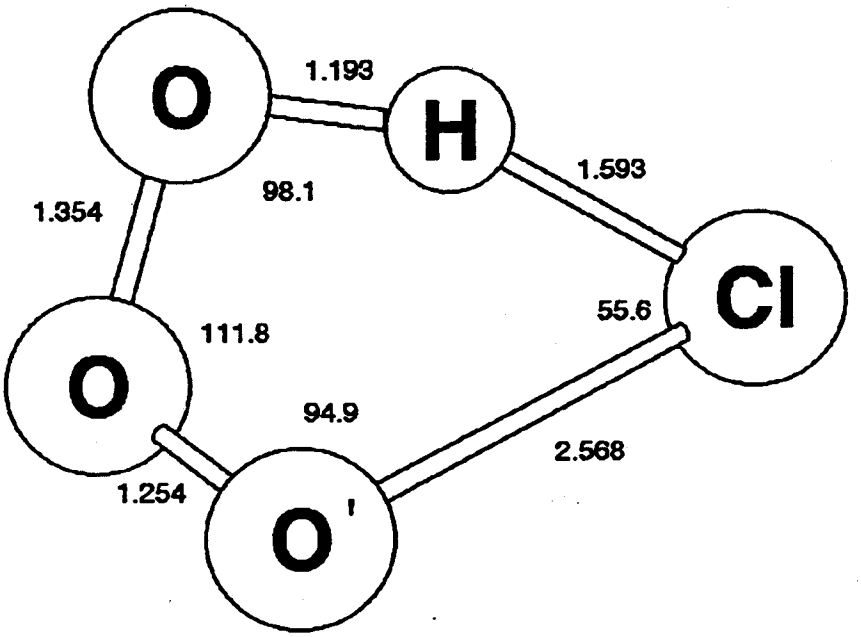

Figure 5c

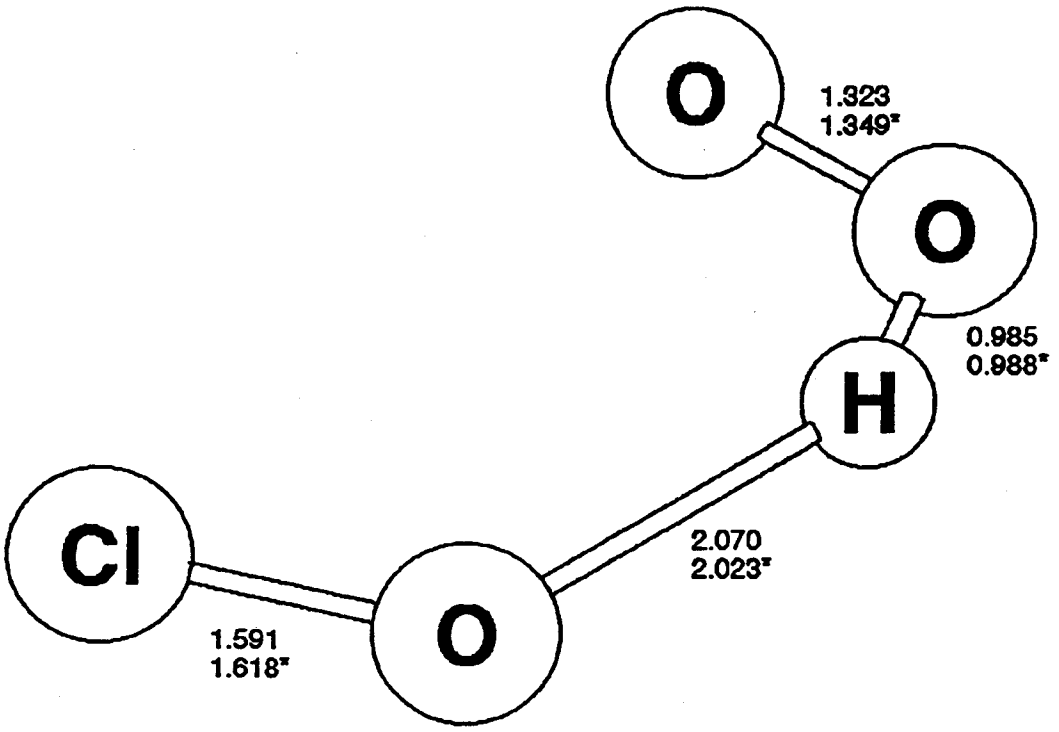

Figure 6a

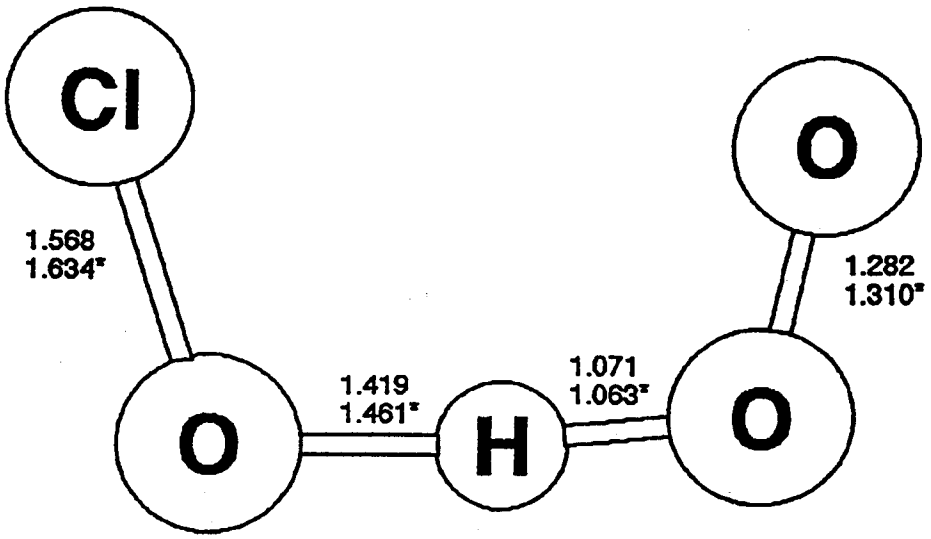

Figure 66

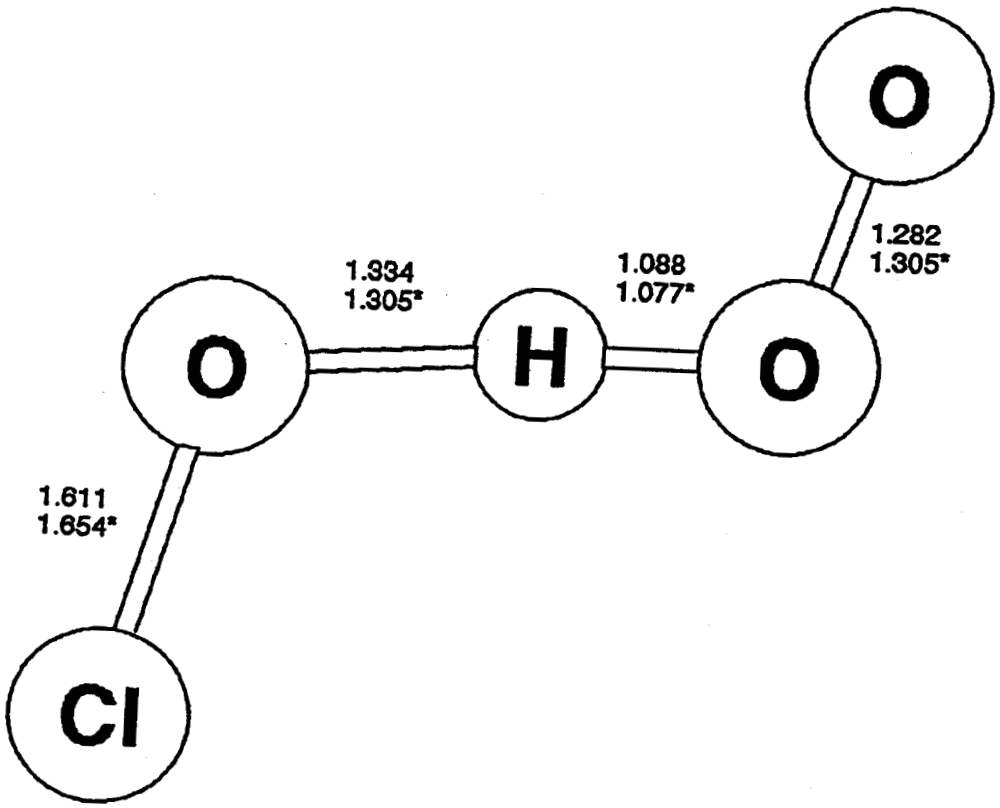

Figure 6C

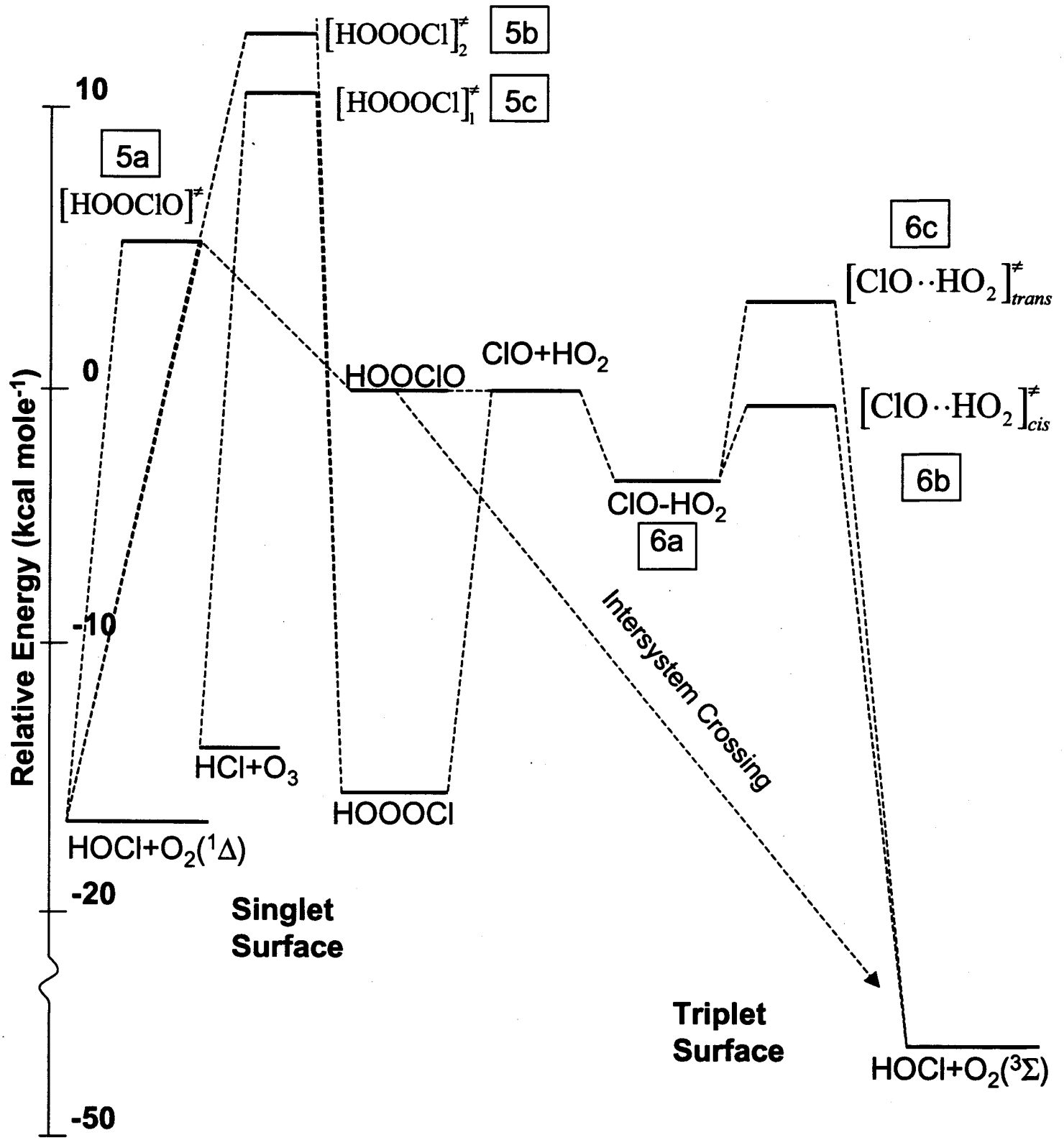
Relative Energy (kcal mole-1)
10
0
-10
-20
-50
5a
[HOOClO]≠
[HOOOCl]2≠ 5b
[HOOOCl]1≠ 5c
HOOClO
ClO+HO2
ClO-HO2
6a
6c
[ClO··HO2]≠trans
[ClO··HO2]≠cis
6b
HCl+O3
HOOOCl
HOCl+O2(1Δ)
Singlet Surface
Intersystem Crossing
Triplet Surface
HOCl+O2(3Σ)

Figure 7

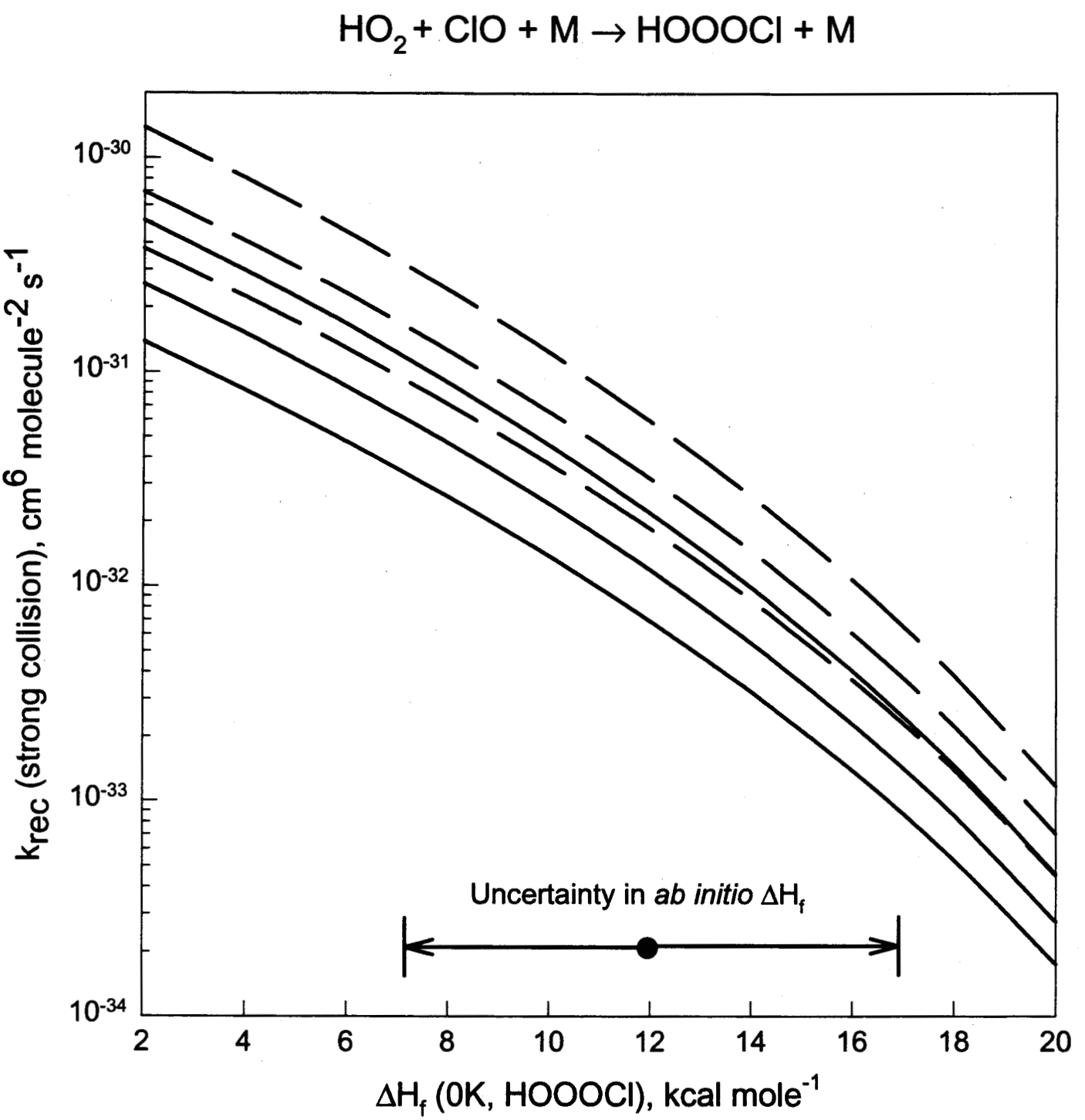
$HO_2 + ClO + M \rightarrow HOOOCl + M$
k_{rec} (strong collision), cm^6 molecule^{-2} s^{-1}
10^{-30}
10^{-31}
10^{-32}
10^{-33}
10^{-34}
Uncertainty in *ab initio* ΔH_f
2
4
6
8
10
12
14
16
18
20
ΔH_f (0K, HOOOCl), kcal mole^{-1}

Figure 8